EFFECTS OF COLLAGEN POST-TRANSLATIONAL MODIFICATIONS ON BONE DENSITY AND MECHANICAL PROPERTIES IN OSTEOGENESIS IMPERFECTA

Master Thesis Biomedical Engineering
9 December 2018

Author
Name: Stefan Smit

Supervisors
prof.dr.ir. H.H. Weinans | TU Delft
dr.ir. B. Pouran | UMC Utrecht
W.H. Nijhuis, MD | WKZ Utrecht

TU Delft

Wilhelmina Kinderziekenhuis

Abstract

Osteogenesis imperfecta (OI), also known as brittle bone disease, affects 1 in 10.000 births. This disease is characterized by skeletal dysplasias, bone fragility and many secondary health issues. It is a heritable disorder affecting collagen type I, which is an essential protein in bone tissue. Post-translational overmodifications in collagen biosynthesis disturb the collagen packing and alter the mineralization process. This results in bone with poor structural parameters and inferior mechanical properties. In the current study, we have tested the hypothesis that the structural and mechanical properties in bone samples from OI patients are related to altered post-translational modifications in the collagen molecules.

Hydroxylysine (Hyl) and the crosslinks hydroxylysyl-pyridinoline (HP) and lysyl-pyridinoline (LP) in bone samples from OI patients were measured with liquid chromatography. Bone quantity, in terms of volumetric bone mineral density (vBMD) and volumetric tissue mineral density (vTMD), was measured with micro-computed tomography. Hardness and Young's moduli were derived from indentation experiments.

Lysine was overhydroxylated in OI bone ($p < 0.001$), which led to increased HP values ($p < 0.001$) and higher HP/LP ratios ($p = 0.013$) compared to controls. OI tissue mineral density was more heterogeneously distributed, although average vTMD values were similar in both groups. The vBMD was significantly higher in controls compared to OI bone samples. Elevated Hyl levels were significantly related to decreased vBMD and vTMD in bone samples from OI patients. In both OI and control samples, an increase in LP crosslinks was associated with elevated vTMD values. Indentation with a spherical tip ($r = 0.25$mm) showed no altered mechanical properties in OI compared with controls. Unfortunately, we could not determine if impaired overmodifications in collagen are related to the poor mechanical properties of OI bone. Young's moduli and hardness were not related to HP levels or HP/LP ratios. In control bone samples a negative correlation between Hyl residues and mechanical properties is observed. More mechanical experiments are necessary to address the hypothesis appropriately.

Table of contents

1. Introduction

Osteogenesis imperfecta (OI) is a group of genetic disorders, affecting different connective tissues in the body. The disease is characterized by skeletal dysplasia's and bone fragility, explaining the generally used terminology 'brittle bone disease'. Prevalence is estimated in 1 per 10.000 births. Distinctive types exist and classification is based on a combination of genotype and phenotype. This study is addressed to types with mutations in the COL1A1 or COL1A2 genes, which encode collagen type I α-chains. In 85% of all OI patients, this is the origin of the disease (Marini et al., 2017). Sillence et al. introduced a classification of these types based on clinical appearance, such as color of sclerae, body stature and bone deformity (Sillence et al., 1979). Type I is the mildest form and type III is the most-severe, non-lethal class. Patients encounter many secondary health issues like hearing loss, respiratory complications and gastrointestinal problems. An intermediate group is type IV. Patients with OI type II decease in the perinatal period.

The pathophysiology of osteogenesis imperfecta is unclear. There is no cure and treatment is based on physiotherapy, fracture repair by orthopedic surgery and rehabilitation. Bisphosphonates are applied as drug treatment in clinics to enhance bone formation and reduce fracture risk (Sakkers et al., 2004; Rijks et al., 2015). However, this therapy suppresses only one single factor of all symptoms that could occur in OI. Aim of this research is to gain more insight in the mechanisms behind this disease, which will hopefully lead to better treatments to increase the quality of life of patients diagnosed with OI.

During daily activities, bones in the human body experience various forces and microfractures arise continuously. A sufficient amount of bone tissue with a certain quality is necessary to withstand those different loading conditions. **Figure 1** shows different factors affecting the quantity and quality of bone tissue and thereby the bone strength. In osteogenesis imperfecta, many impairments in bone tissue are observed. These findings will be discussed shortly in the sections below.

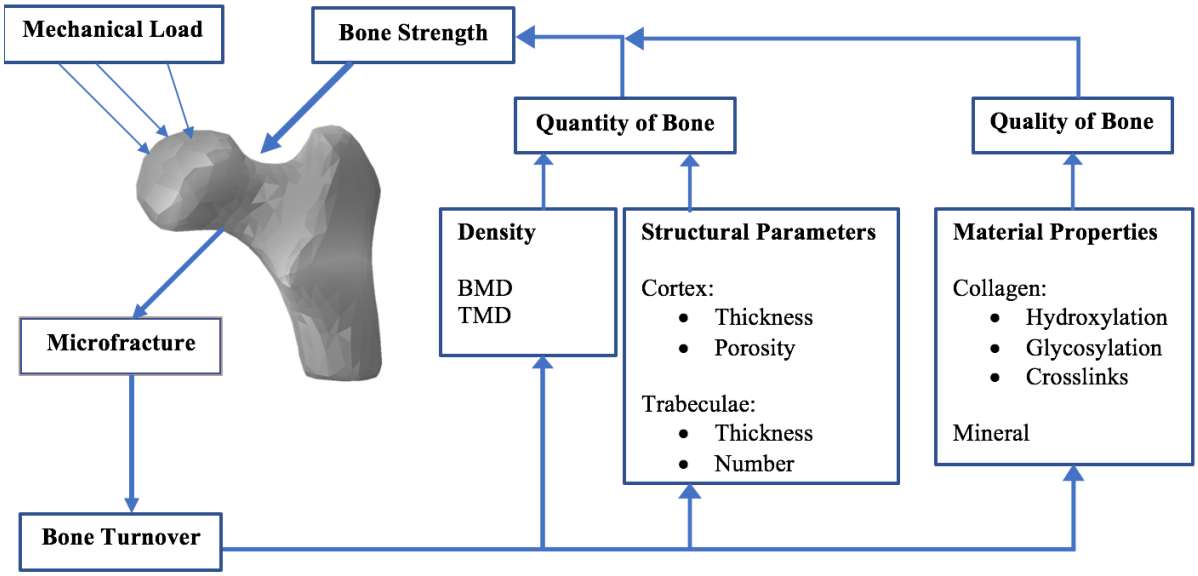

Figure 1. *Flow diagram of the main factors influencing bone strength. Bones are loaded during routine activities and microfractures arise. Different types of bone cells collaborate to resorb the damaged site and create new bone tissue. A functional collagen scaffold combined with a correct mineral deposition determines the quality of bone material. At tissue level, bone density and microstructural parameters as cortical thickness and porosity determine the amount of bone tissue. Impairment of any of these factors has consequences on the mechanical behavior of bone tissue.*

1.1 Quantity of bone

Bone density is measured in various ways. Dual-energy x-ray absorptiometry (DXA or DEXA) is a diagnostic tool in clinics to identify osteoporotic bone in vivo. Low bone density scores measured with this technique are typical for OI patients. For research purposes, small bone fragments are imaged ex-vivo with micro-computed tomography (μCT) to derive the volumetric bone mineral density (vBMD) and the volumetric tissue mineral density (vTMD). These parameters are single values representing the density in g/cm^3. The vBMD is the average density of all voxels in a selected volume, independent if the voxel is associated with bone tissue or an intracortical pore. The vTMD however, includes only bone tissue by segmenting out all voxels which are below a pre-defined threshold. This strategy excludes pores and determines the average density of the bone tissue. By definition, vTMD will be higher than (or equal to) the vBMD.

Structural parameters as cortical thickness and porosity are therefore important factors for the vBMD. Bone tissue from OI patients is known for its poor structural parameters. Cortical thickness, trabecular number and trabecular thickness were all decreased in OI types I, III and IV (Baron et al., 1983; Ste-Marie et al., 1984; Rauch et al., 2000; Roschger et al., 2008). Furthermore, abnormal high intracortical porosity is observed (Jameson, 2014; Imbert et al., 2015; Albert et al., 2017; Blouin et al., 2017). Hence, values for vBMD are low compared with healthy controls (Jameson, 2014; Imbert et al., 2015; Albert et al., 2017). This intracortical porosity correlates negatively with the poor mechanical properties of OI bone (Albert et al., 2014; Vardakastani et al., 2014). For this reason, bisphosphonate treatment is employed in OI patients to improve bone structural parameters and increase the vBMD. This intervention is based on obstruction of bone resorption by osteoclasts rather than improved bone formation by osteoblasts (Bishop, 2016). When results are compared in literature, researchers should be aware if patients received bisphosphonates.

At micro scale, it is generally accepted that bone tissue of OI measured by backscattered electron imaging, is hypermineralized (Boyde et al., 1999; Roschger et al., 2008; Fratzl-Zelman et al., 2014). Therefore, the mineralization of OI bone at tissue level, the vTMD, is expected to be higher than controls. This was indeed observed by Imbert (2015), although no significant differences were found by Albert (2017). Bisphosphonates were part of the medical therapy of the examined OI patients. The effects of this drug treatment to vTMD are unclear.

1.2 Bone mechanical properties

From clinical appearance, it is clear that mechanical properties of bone tissue from OI patients are inferior to normal healthy bone. Three-point bending experiments demonstrated a lower Young's modulus, yield strength and bending strength in OI type III compared with controls (Albert et al., 2017). Compression of hydrated bone samples showed significantly lower Young's modulus, yield stress and ultimate stress. None of the mechanical properties correlated with vTMD in OI bone (Imbert et al., 2015).

Furthermore, nano-indentation tests with atomic force microscopy were performed in numerous studies to characterize the mechanical properties of mineralized collagen fibrils. Young's modulus was lower in bone samples from OI samples compared with healthy control bones, but the modulus was highly correlated with vTMD (Imbert et al., 2014). However, a different study encountered higher Young's moduli and hardness in OI versus controls (Weber et al., 2006). Patients with OI type I had higher elastic modulus and hardness than patients with OI type III in nano-indentation experiments (Albert et al., 2013), which is unexpected as a higher mineralization density is found in patients with OI type III than type I

(Boyde et al., 1999). Legitimacy of this comparison is open for debate as Boyde et al. don't mention if OI patients received bisphosphonate therapy. However, the use of bisphosphonates to increase bone density was not a widespread phenomenon at the time the researchers published their findings. These contradictions might also occur due to heterogeneity of bone tissue at this small scale. This is supported by (Katti et al., 2016) who concluded that nano-mechanical properties vary over the anatomical positions in one human OI bone sample.

1.3 Quality of bone

The quality of bone tissue has major influence on the mechanical properties of bone at organ level. Bone tissue behaves as a biphasic composite material, where the collagen matrix gives bone its mechanical toughness and the inorganic hydroxyapatite (HA) phase increases the stiffness. Collagen molecules are interconnected with crosslinks to create long collagen fibrils, which become mineralized. HA covers the circumference and occupies intrafibrillar spaces between collagen molecules. The mineral-to-matrix ratio, describing the amount of mineral per amount of organic matrix, was significantly higher in OI. This higher ratio had a negative effect on the mechanical properties of the bone tissue measured by nanoindentation (Imbert et al., 2014). A different study found similar mineral-to-matrix ratios compared to controls (Paschalis et al., 2016). Collagen synthesis will be discussed in more detail using **Figure 2.**

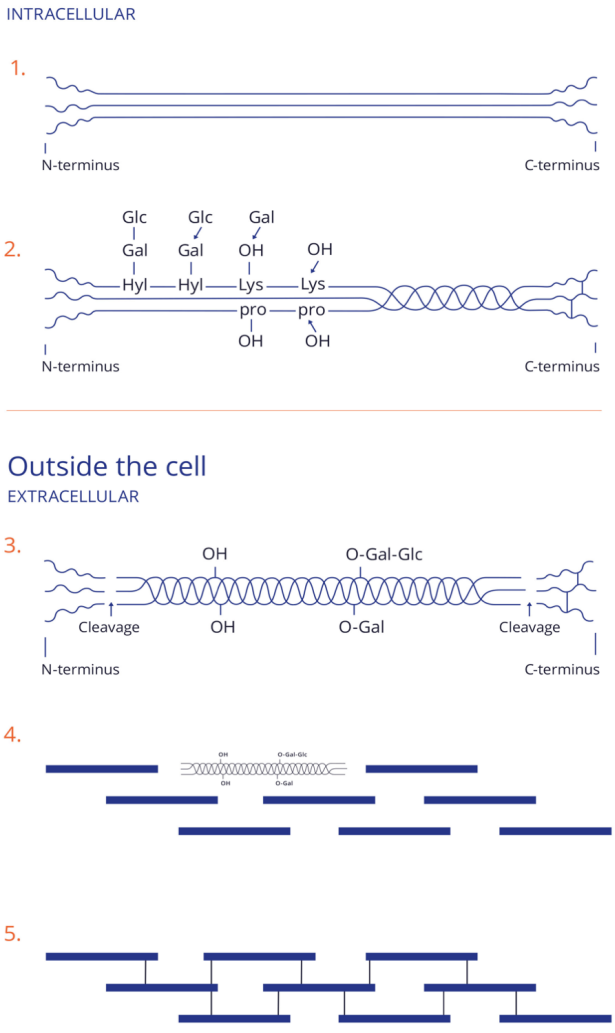

Figure 2. *Brief description of collagen synthesis.*
(1) *Collagen type I consists of two α1-chains and one α2-chain, which are translated from the mRNA inside the cell.*
(2) *Trimerization of the α-chains takes place at the C-terminus and the triple helix is formed through a zipper-like mechanism towards the N-terminus. Simultaneously, enzymes perform post-translational modifications. Proline (Pro) and lysine (Lys) are hydroxylated and hydroxy-lysine (Hyl) is glycosylated by consecutively galactose (Gal) and glucose (Glc).*
(3) *After secretion in the extracellular space, the propeptides at the C- and N-terminus are cleaved off. The remaining mature collagen molecule consists of a long triple helical section flanked by short unwinded telopeptides.*
(4&5) *Individual collagen molecules align and are interconnected by crosslinks to form long collagen.*

Genes for pre-procollagen chains are transcribed in the cell nucleus in a repeating [Glycine(Gly)-X-Y]$_n$ pattern where X and Y can be any amino acid, although proline (Pro) is very common (Ramshaw et al., 1998). These mRNA chains migrate out of the nucleus into the cytoplasm where they are translated by ribosomes to procollagen α1- and α2-chains (**1**). Subsequently, post-translational modifications (PTMs) are carried out by the rough endoplasmic reticulum and are necessary for correct triple helix formation and fibrillogenesis. Two α1-chains and one α1-chain align and trimerize at the propeptides of the C-terminal (**2**). Folding of the α-chains to a triple helix is initiated and propagates, guided by enzymes, through a zipper-like mechanism towards the N-terminus (Boudko et al., 2012).

Meanwhile, other modifications like hydroxylation and glycosylation occur. Proline (Pro) and lysine (Lys) residues are hydroxylated by enzymes and are converted to hydroxyproline (Hyp) and hydroxylysine (Hyl) respectively. During glycosylation, the carbohydrates galactose and glucose attach to the Hyl residues. The physiological role of this step is unclear. Both the hydroxylation and glycosylation are enzymatic reactions and continue until the chains are twisted into a helical conformation and the enzymes cannot perform their task anymore. The procollagen molecules are secreted into the extracellular space and the propeptides are cleaved of (**3**). Different collagen molecules align (**4**) and are enzymatically interconnected by crosslinks (**5**). This is a stepwise mechanism in which an immature divalent crosslink connects two adjacent collagen molecules first. A fraction of these immature crosslinks reacts spontaneously with a third collagen to form a mature trivalent crosslink.

The only suitable attachment sites in collagen molecules for crosslinking are Lys and Hyl residues in both the telopeptides and the helical region. The amino acid which is used for the reaction (Lys or Hyl) combined with its molecular location (telopeptidyl or helical) determines the type of crosslink. Different combinations are shown in **Figure 3**. Two classes of mature crosslinks exist: the pyridinoline (HP and LP) and the pyrrole (HPL and LPL) crosslinks. There are already indications that crosslinking is related to mechanical properties of bone (Saito and Marumo, 2015) and further research is valuable. Pyrroles are not fluorescent by nature and are more difficult to detect. Most research regarding enzymatic crosslinking in bone is for that reason addressed to pyridinoline measurement.

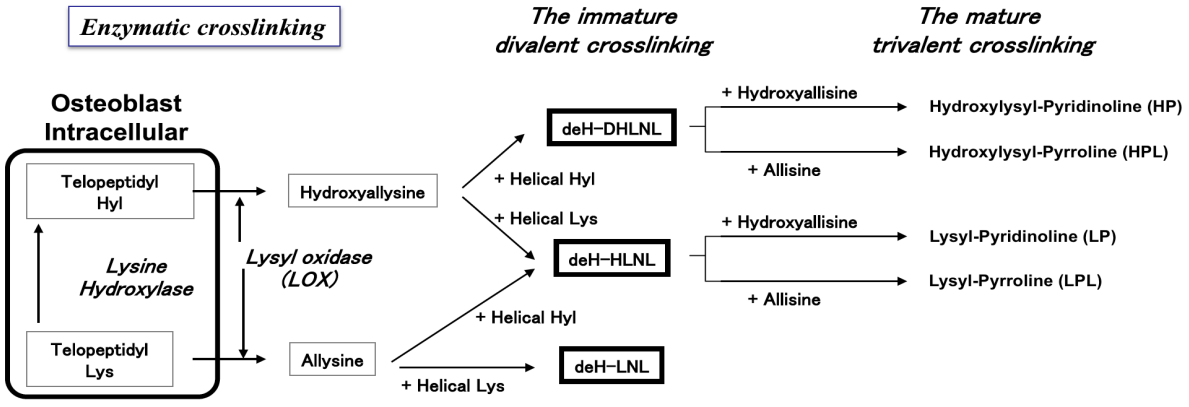

Figure 3. *Detailed description of enzymatic crosslinking in fibrillar collagens. The hydroxylation of telopeptidyl is regulated by intracellular lysine hydroxylase (LH) enzymes and is tissue specific. Extracellular lysyl-oxidase (LOX) enzymes control the total amount of crosslinks by conversion of telopeptidyl Lys and Hyl to their aldehyde structures allysine and hydroxyallysine. Immature crosslinks are formed by a spontaneous condensation reaction between the aldehydes and helical Hyl or Lys. Trivalent crosslinks are established by binding a third aldehyde Lys or Hyl residue. Abbreviations: deH-DHLNL dehydro-dihydroxylysinorleucine, deH-HLNL dehydro-hydroxylysinorleucine, deH-LNL dehydro-lysinonorleucine. Obtained from (Saito and Marumo, 2015) and names of the mature trivalent crosslinks are edited to match with the terminology used in this paper.*

Overhydroxylation of lysine in collagen type I in OI patients is detected frequently. This is demonstrated in OI bone tissue (Kirsch et al., 1987; Bank et al., 2000), dermis tissue (Petrovic and Miller, 1984) and cell cultures of skin fibroblasts (Kirsch et al., 1987; Lehmann et al., 1995). Considering the enzymatic crosslinks in bone tissue, an increase in HP was found. LP was not significantly different, so an increase in HP/LP ratio and total pyridinoline crosslinks (HP +LP) was determined. This finding matches with an increase in Hyl. No relationship was determined in HP/LP ratio over age or OI classification (Bank et al., 2000).

Lysyl-hydroxylation is exclusively an intracellular process during collagen synthesis and is important in crosslink formation. The difference between the formation of HP and LP depends on the crosslinking of a triple helical Hyl or Lys. Measurement of both amino acids will provide information about the extent of lysine hydroxylation. Before hydroxylation, a fixed amount of 107 Lys residues are part of collagen type I molecules. Lysine is in contrast to its hydroxylated counterpart a common component of several proteins and proteoglycans and the origin of lysine cannot be distinguished with the protocols applied in this study. For this reason, only detection of Hyl will be used as a measure for hydroxylation. Furthermore, crosslinking in OI bone tissue is explored by HP and LP measurements. The amount of collagen per mg dry-weight bone is estimated by the detection of hydroxyproline. Hyp is very tissue specific and each collagen type I molecule contains in general 300 residues. These biochemical assays are performed with liquid chromatography.

It is clear that a reduced quantity of bone contributes to the weak mechanical properties observed in OI bone. However, there is a lack of knowledge about the quality of bone tissue of OI patients. Biochemical assays with liquid chromatography are performed to determine: (i) the amount of collagen per mg bone (ii), the hydroxylation of lysine (iii) and to measure the pyridinium crosslinks. Young's modulus and hardness of the bone samples are obtained by indentation experiments to check if correlations with biochemical parameters exist. In addition, vBMD and vTMD are obtained by μCT imaging as measures for bone density. More specifically, we tested if modifications at the collagen molecular level correspond to the structural and mechanical properties measured by μCT and indentation experiments. We hypothesize to observe the following findings:

1. Lysine in collagen type I in bone tissue from OI patients is overhydroxylated, which leads to more HP crosslinks and increased HP/LP crosslink ratio's.
2. Hypermineralization in OI bone is evident by a lower collagen content and increased vTMD values.
3. The amount of bone tissue per volume, the vBMD, is decreased in OI bone.
4. Impaired crosslinking and altered vBMD and vTMD values in OI bones are correlated with reduced hardness and Young's moduli.
5. Parameters are more evident in severe OI type III than in OI type I and IV.

The opportunity to perform biochemical, mechanical and imaging analysis all on the same bone fragment of each individual OI patient, is rarely done and will definitely contribute to more knowledge about the pathogenesis of osteogenesis imperfecta.

2. Materials and Methods

2.1 Patients and sample collection

Bone specimens were collected over a period of more than twenty years from children who underwent orthopedic surgery at Wilhelmina Children's Hospital (Utrecht, the Netherlands). Most surgical interventions were performed to treat skeletal dysplasias. Bone fragments, which were removed from the patient for medical reasons during surgery, were declared as post-surgical waste material and stored for scientific purposes.

Waste material was anonymized and without any additional preparations stored for future research in containers at -80°C within 24 hours after surgery. The specimens were categorized as 'control bone' or 'OI bone'. For this research, only specimens originating from long bones of the lower extremities, i.e. femur, tibia and fibula, were included. Many different types of OI are identified and the list is growing. Types which do not arise from a genetic defect in the COL1A1 or COL1A2 are excluded. This leaves an OI group (n=19) with type I (n = 1), III (n = 13) and IV (n = 5) and a control group with 24 specimens. All OI patients received bisphosphonate treatment. A detailed description of patient characteristics is provided in **Appendix A**.

Specimens were treated in such a way to minimalize the number of thaw/freeze cycles. When the samples were retrieved from the freezer, they were directly placed in a closed Styrofoam box with dry ice. Of each specimen, three fragments of cortical bone were cut off using a stainless-steel nipper. For biochemical analyses, size of the bone fragment was not relevant and a piece of a few millimeters was sufficient for both amino acid and crosslink analysis. Experiments regarding μCT and indentation were performed on the same bone fragment. Bone samples need to be flat and stable for proper indentation experiments. Cortical fragments, approximately 5x10 mm, with only a minor curvature of the surface are collected. Trabecular bone and other tissues were removed. If the whole bone specimen was too small or no smooth cortical surface was available, no fragment was taken for mechanical experiments. Samples were stored at -20°C until use.

2.2 Biochemical analysis

Liquid chromatography (LC) is an analytical separation technique based on a liquid mobile phase flowing through a solid stationary phase. Tissue samples are cleaved into small molecules by hydrolyzation and are dissolved in a solution. Identification of different compounds is based on the affinity of the molecules with the mobile and stationary phase. High performance liquid chromatography (HPLC) is used very often in analytical chemistry. A schematic set up of HPLC is shown in **Figure 4**. If experimental parameters are chosen correctly, the chromatogram shows separated peaks in which every peak is a measure for the number of molecules from a single compound passing the detector (**Figure 5**). Quantification of the compound is done by calculating the area under the curve of each peak.

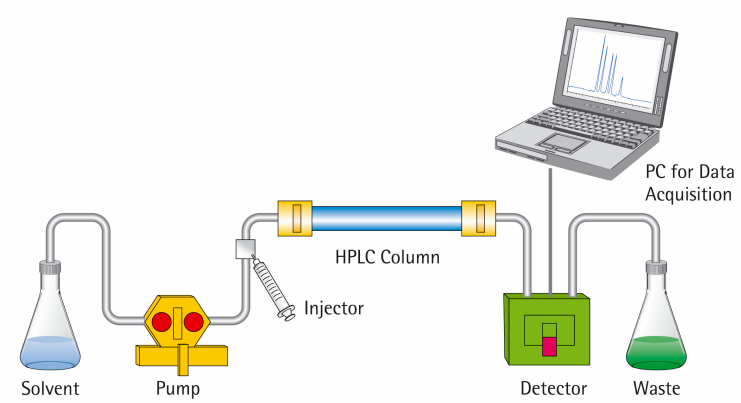

Figure 4. *Typical set up for HPLC measurements. A pump increases the pressure of the solvent (the mobile phase) and the sample is injected. The stream passes a HPLC-column (the stationary phase). This column is packed with adsorbent material with specific chemical properties. Some molecules of the sample are attracted to the packing material of the column and slow down while others have more affinity with the mobile phase and are rapidly flushed away. The time it takes for a compound to pass through the column is called the retention time. When molecules leave the column, they are detected by a UV or fluorescence detector. The results are visualized in a chromatogram.*

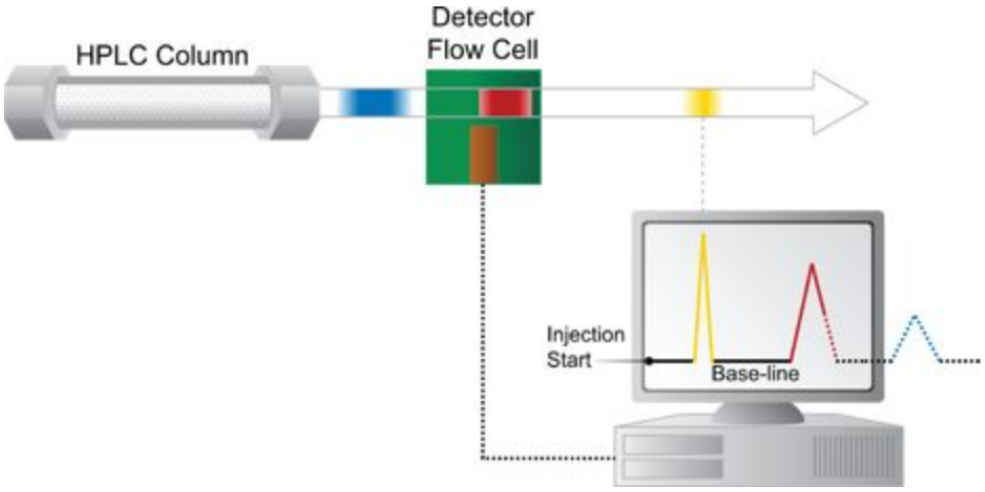

Figure 5. *Continuation of the HPLC system of Figure 4. The yellow compound is not attracted by the packing material of the stationary phase and leaves the HPLC column with only a small delay. The first peak in the chromatogram corresponds therefore to the yellow compound. The blue compound is attracted the most by the stationary phase and needs more time to leave the column. This corresponds to the last peak in the chromatogram. Obtained from http://www.waters.com/waters/en_NL/How-Does-High-Performance-Liquid-Chromatography-Work%3F/nav.htm?cid=10049055&locale=en_NL date: October 1st, 2018*

Developments in HPLC equipment resulted in ultra-performance liquid chromatography (UPLC) instruments. UPLC columns are shorter and are packed with particles less than 2.0 µm, where HPLC columns are normally packed with 3-5µm particles. These improvements allow better resolution and sharper peaks (Gumustas et al., 2013) and UPLC is often preferred over HPLC. A validated UPLC methodology is already developed for crosslink analysis (Sroga and Vashishth, 2011). In our research group, a reliable HPLC protocol for amino acid analysis (Bank et al., 1996) is used repeatedly with complete satisfaction. Therefore, this method is carried out again.

Before biochemical analysis, the bone samples need to be cleaned thoroughly to remove non-bone tissue. Dehydration is performed with lyophilization to obtain fully dry bone tissue composed of mineralized collagen. Then, the structure and macromolecules are completely partitioned in individual amino acids, crosslinks and other small molecules by acid hydrolyzation to enable molecular separation by liquid chromatography. These steps are described more comprehensively in **Appendix B**.

2.2.1 HPLC method for amino acid analysis

Amino acids Hyp and Hyl are separated and quantified based on the method proposed by (Bank et al., 1996). Assuming 300 Hyp residues per collagen molecule, the amount of collagen in the sample is calculated. The amount of Hyl provides information about the degree of hydroxylation during collagen synthesis. Quantity of Hyl is expressed as moles per mole collagen.

Measurements were performed on an Alliance 2795 Seperations module (Waters Corporation, Milford, MA, USA) in series with an Alliance 2475 Multi Fluorescense detector (Waters Corporation, Milford, MA, USA) with excitation and emission wavelengths of 254nm and 630nm respectively. A Tosoh TSKgel ODS-80-TM column (4.6mm internal diameter x 15.0cm) packed with C_{18} coated silica particles is used for reversed-phase chromatography. Data analysis was performed with Waters Empower 3 Chromatography Data Software. Column temperature was kept constant at 30°C and the samples at 20°C. Initial system pressure before sample injection (50µl) was 1790 psi with a steady pressure ripple between 15-20 psi. The run time for one sample was 40 minutes with a constant flow rate of 1.4 ml/min. Three different eluents were used for HPLC analysis. Solvent A and B are acidic citrate solutions with different pH values and solvent C is 100% acetonitrile. The injection needle was washed after every injection with 10% methanol. When the experiment was finished, the column is washed and stored in 100% acetonitrile. **Appendix C** provides a complete description of required chemicals, preparations for reagents and chromatographic conditions.

After hydrolyzation, bone sample residues for amino acid analysis are dissolved (50µl per mg dry weight) in a 24µM homoarginine internal standard (IS) solution. This IS does not interfere with other substances in the chromatogram and is used to compensate for small mixing errors during sample preparation. A derivatization step with FMOC is performed to enable amino acid detection with the fluorescence detector.

External standards were prepared for calibration. Each standard contained different amounts for Hyp and Hyl. A calibration curve was fitted over a range of 3-60µM for Hyp and a lower range (0.6-12 µM) was selected for Hyl calibration. The external standard with the highest concentration is made and diluted to lower concentrations, to minimize the risk of mixing errors of individual concentrations.

2.2.2 UPLC method for crosslink analysis

Collagen molecules form long fibrils by intermolecular crosslinks. In this study, the pyridinoline crosslinks HP and LP are measured with UPLC. Objective of this experiment is to determine the HP/LP ratio and the amount of crosslinks per collagen molecule.

Chromatography is performed with Acquity UPLC M-Class System combined with an Acquity UPLC Fluorescence Detector for the detection of crosslinks (excitation 297nm, emission 395nm). An Acquity UPLC BEH C18 column (2.1 mm internal diameter x 50mm) was used for crosslink separation and the column was guarded by a Acquity UPLC BEH C18 VanGuard pre-column, (2.1 mm internal diameter x 5 mm). Data analysis was performed withEmpower 3 Chromatography Data Software. All systems and complementary accessories are obtained from Waters Corporations (Milford, MA, USA).

Starting composition of the solvents was 90% solvent A and 10% solvent B. Separation of the crosslinks was achieved by a linear gradient from 10% of solvent B to 20.5% over the total analysis time of 5 minutes. Solvent A contained 0.12% (v/v) HFBA in MQ water and solvent B was a mixture of solvent A with acetonitrile in a 1:1 (v/v) ratio.

Injection volume was 5 µl and the column was washed for 2 minutes between samples with the starting composition of 90% eluent A.

Bone residues from acidic hydrolyzation are dissolved in 1 ml internal standards solution. This solution contains 1 µM pyridoxine (the internal standard) in 1% (v/v) HFBA in 10% (v/v) acetonitrile. The samples are vortexed rigorously, centrifuged for five minutes and aliquots of 100µl of clear supernatant were used for UPLC measurement.

An external standard containing both HP and LP was obtained from Quidel Corporation. An external calibrator is prepared with 30% (v/v) HP&LP standard, 1% (v/v) HFBA in 10% (v/v) acetonitrile. This solution is diluted several times to obtain a calibration curve over 0.35 - 4.1 µM range for HP and 0.19 - 2.2 µM range for LP. A complete description of the protocol is stated in **Appendix D**.

2.3 Imaging with micro-computed tomography

Micro-computed tomography is used to determine the vBMD and vTMD of control and OI bone. As described in section 2.1, trabeculae and other tissues were removed by hand from the sample and no other (chemical) cleaning step was performed.

For calibration, five hydroxyapatite phantoms with increasing density (0.25, 0.50, 0.75, 1.00 and 1.25 g/cm^3) are used. These phantoms are taped with an equidistant spacing around the periphery of an Eppendorf. A bone sample is placed in the same Eppendorf, close to the phantoms. Next, the Eppendorf is cooled by placing it in a 50 ml Greiner tube filled with dry ice to prevent the tissue from complete thawing. This tube is positioned horizontally in a Quantum FX micro-CT scanner from PerkinElmer (Waltham, MA, USA) and monitored to verify that there is no overlap between sample and phantoms in radial direction. Finally, the samples were scanned for two minutes at 90 kV and 200 µA with a resolution of 30 µm.

After image acquisition, the stack of images was converted to a 16-bit TIFF-file for analysis with ImageJ (NIH, Redwood Shores, CA, USA). Average grey values of the phantoms were determined with a circular region of interest through as many slices as possible, generally around 80 slices. With these values, the complete file is converted to hydroxyapatite densities. In addition, the microscopic structure of the samples is observed with µCT images. Woven bone is characterized by a disorganized extracellular matrix and is mechanically weak. This type of bone is produced rapidly by osteoblasts as a first stage for fracture repair, before it remodels to more organized and strong lamellar bone.

Data analysis was performed with a custom Matlab-script (MATLAB, Mathworks, version R2016b), **Appendix E**. Based on the TIFF-images, HA values higher than 1700 g/cm^3 are determined as artefacts from beam hardening, or metal remnants from surgery and are therefore ignored. A minimum HA value of 0 g/cm^3 is chosen to determine the vBMD. To compute the vTMD, porosity needs to be excluded. A threshold value of 0.85 g/cm^3 is necessary to be identified as bone tissue. vBMD and vTMD are calculated from the mean HA density of all voxels within the predefined range.

The density distributions of the voxels of the control samples and OI samples are constructed with a free-of-charge function ‘boundedline.m’ from the file-exchange website of Mathworks, provided by Kelly Kearny, version 1.4.0.0. The diagrams show how many times the density of each voxel is counted, normalized to the total amount of measured voxels.

2.4 Indentation

Mechanical indentation was performed after μCT imaging on the same bone samples. Aim of this part is to deduce the Young's modulus and hardness from load-displacement curves. Experiments are carried out with a Lloyd LR5K testing machine (Lloyd Instruments, Bognor Regis, UK) equipped with a stainless-steel (ν_i = 0.30, E_i = 200 GPa) indenter head and a 5N load-cell. The indenter had a spherical tip with radius (*r)* of 0.25 mm. The extension resolution of the instrument was < 1 micron.

Because of biosafety regulations, the complete set-up is wrapped in transparent plastic household foil. Indentation was performed on cortical bone at the anatomical external side. Remnants of trabeculae are removed by fine abrasive paper to rule out mechanical failure of loose tissue particles during the measurement. The experiment is performed on bone samples immersed in phosphate buffered saline (PBS) at ambient temperature. Loctite Super Glue is applied to prevent the sample from floating. Each sample was tested at three random locations of the bone surface. The distance between the cutting edge and the measurement location was approximately 2 mm. Similar spacing were used between individual measurements on the same sample.

Initially, our protocol was based on the paper from (Kerrigan et al., 2014), which is adjusted by trial and error. A piece of short fiber filled epoxy (Sawbones, Vashon Island, WA, USA) simulated cortical bone to test our protocol. Before each measurement, the indenter is lowered until the load cell registered 0.02 N, indicating that the indenter and bone are in contact. Subsequently, the indenter moves upward until the force drops to 0. This will be starting point for indentation. If the load cell shows a value of 0.1 N or higher, the indenter was lowered too quick and the bone surface was penetrated too much. In that case, a new location was chosen. Indentation was performed at 0.05 m/s to a depth of 0.1 mm and holds for 40 seconds. This displacement-controlled protocol was defined in Ondio software (Chatillon Fore Measurement, Largo, FL, USA). Stress relaxation reaches a plateau in this period. Then, unloading was performed at 0.05mm/s. Over the whole indentation trajectory, 1000 data points are extracted for evaluation of the results with a custom-made Matlab script (MATLAB, Mathworks, version R2016b), which is provided in **Appendix F**.

Computation of the reduced Young's modulus *E* and hardness is based on the unloading curve in a load (*P*) – displacement (*h*) diagram, using the Oliver-Pharr method (Oliver and Pharr, 1992). First, the tangent of the slope at the max penetration depth h_{max} during unloading is derived. This is the elastic unloading stiffness *S*:

$$S = \left.\frac{dP}{dh}\right|_{h_{\max}} \tag{1}$$

From which the contact depth h_c is calculated:

$$h_c = h_{\max} - \varepsilon \frac{P_{\max}}{S} \tag{2}$$

where P_{max} is the maximum load before unloading and ε is a geometrical constant and equals 0.75 for a spherical tip (Oliver and Pharr, 2004). The projected contact area A_c of the indenter is a function of h_c:

$$A_c = 2\pi r h_c \tag{3}$$

Equation (4) shows how the reduced elastic modulus E_{eff} is derived with these parameters:

$$E_{eff} = \frac{1}{\beta}\frac{\sqrt{\pi}}{2}\frac{S}{\sqrt{A_c}} \tag{4}$$

where the empirical indenter shape factor $\beta \approx 1$ for a spherical tip. Assuming that no elastic deformation occurs in the indenter, E_{eff} can be converted to the Young's modulus of bone E_{bone} with the following relationship:

$$\frac{1}{E_{eff}} = \frac{1-\nu_{bone}^2}{E_{bone}} + \frac{1-\nu_i^2}{E_i} \tag{5}$$

in which the subscripts i refers to the Poisson's ratio and Young's modulus of the indenter. The Poisson's ratio of bone ν_{bone} is assumed to be 0.3. In addition, the hardness H is calculated by:

$$H = \frac{P_{\max}}{A_c} \tag{6}$$

2.5 Statistical analysis

Statistical analyses are performed using SPSS Statistics, V25 (IBM Corp, Armonk, NY USA). Parameters of interest of individual groups are plotted as histograms to check by eye if the assumption of normality is met. Sample size, skewness and outliers are taken into account. If the assumption is plausible, two groups are compared by Student's t-test and correlations are examined by the Pearson correlation coefficient r. Non-parametrical Mann-Whitney U-test and Spearman's rank correlation coefficient ρ were applied if the assumption of normality was not reasonable. Causality in correlations was determined by simple linear regression. Unless stated otherwise, statistical significance was determined at $p < 0.05$.

3. Results

3.1 Biochemical analysis

HPLC is performed to measure the amino acids Hyp and Hyl, while UPLC is applied to determine the crosslink levels in bone samples. Retention times of the individual compounds and equations of the calibration curves for HPLC & UPLC measurements are provided in **Appendix G**. All the calibration curves have a $R^2 > 0.9$. The results of the liquid chromatography experiments are presented in **Figure 6**. Means from biochemical analysis were not normally distributed in both the control and OI group simultaneously. For this reason, the results are visualized with boxplots and Mann-Whitney U-test is applied to examine comparisons between 'control' (n = 24) and 'OI' (n = 19). The amount of collagen per mg lyophilized bone was significantly higher in control samples than OI samples ($U = 25$, $p < 0.001$). However, the number of Hyl residues per collagen molecule ($U = 35$, $p < 0.001$), HP crosslinks per collagen molecule ($U = 40$, $p < 0.001$), total amount of pyridinoline crosslinks per collagen molecule ($U = 86$, $p = 0.001$) and the HP/LP crosslink ratio ($U = 126$, $p = 0.013$) were significantly increased in bone samples from OI patient compared with controls. LP levels per collagen were similar in both groups ($U = 204$, $p = 0.557$). Medians and interquartile ranges (IQR) are provided in **Appendix G**.

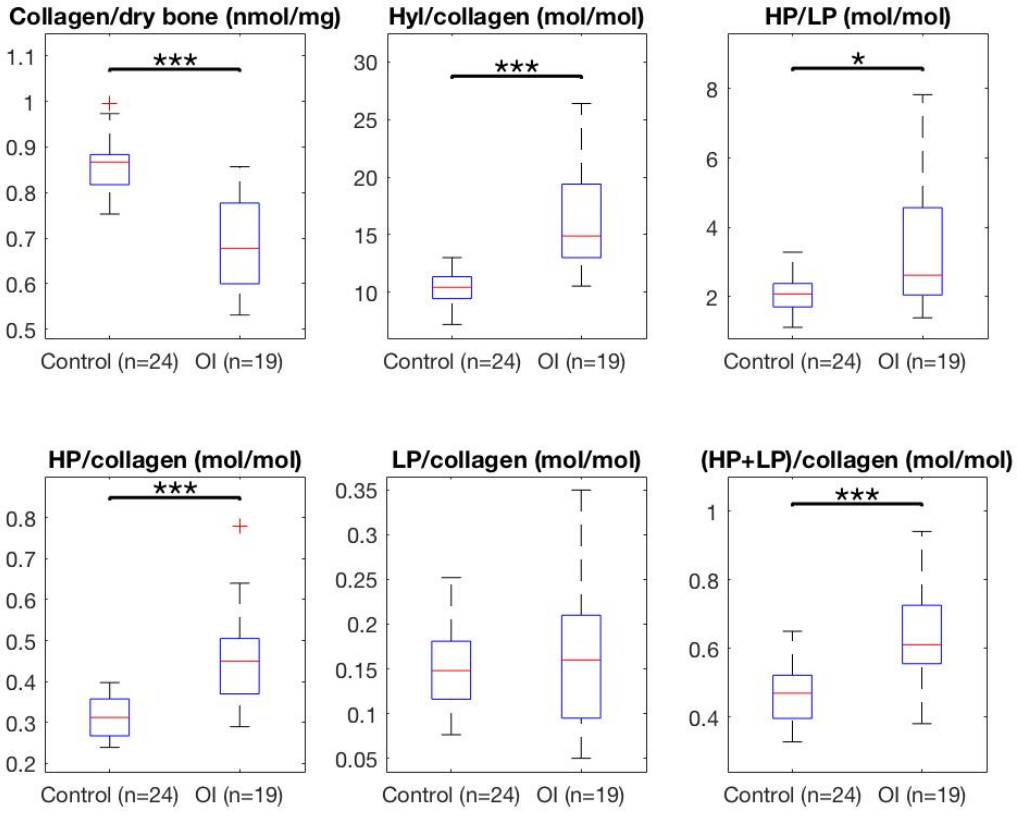

Figure 6. *Bone samples from OI patients and controls are analyzed with liquid chromatography and the results are visualized in boxplots. The amount of collagen per mg dry bone is obtained from Hyp measurements, assuming 300 Hyp residues per collagen molecule. The crosslinks and the number of Hyl residues are normalized per collagen molecule. Statistical significance is tested with the non-parametrical Mann-Whitney U test (* p < 0.05; ***p ≤ 0.001)*

Individual data points of crosslink measurements are plotted against the amount of collagen in each bone sample (**Figure 7A, B, C**). Different colors in the scatterplots are applied to demonstrate differences between OI types. Levels of Hyl are expressed as the

amount of collagen too (**Figure 7D**). Hydroxylation is significantly increased in OI type III compared to controls ($U = 1$, $p < 0.001$) and compared to OI type IV ($U = 5.0$, $p = 0.007$). Hydroxylation was similar in controls and OI type IV ($U = 34$, $p = 0.133$).
Correlations between biochemical parameters are explored with Spearmans ρ. In control bone, significant relationships are found between the amount of collagen in bone and HP levels ($\rho = -0.428$, $p = 0.037$) and between hydroxylation and the crosslink ratio HP/LP ($\rho = 0.451$, $p = 0.027$). Furthermore, the amount of collagen per dry weight bone decreases by age ($\rho = -0.537$, $p = 0.007$).

In OI bone, significant negative relationships were observed between the amount of collagen and (i) HP/collagen ($\rho = -0.477$, $p = 0.039$), (ii) LP/collagen ($\rho = -0.544$, $p = 0.016$) and (iii) the total amount of crosslinks (HP+LP)/collagen ($\rho = -0.647$, $p = 0.003$). No significant relationships were found between biochemical parameters in the OI type III group. LP levels increase significantly with age ($\rho = 0.679$, $p = 0.001$), but this relationship was not observed with HP. HP/LP ratio decreases with age ($\rho = -0.577$, $p = 0.010$) and the total amount of crosslinks increases with age ($\rho = 0.562$, $p = 0.012$).

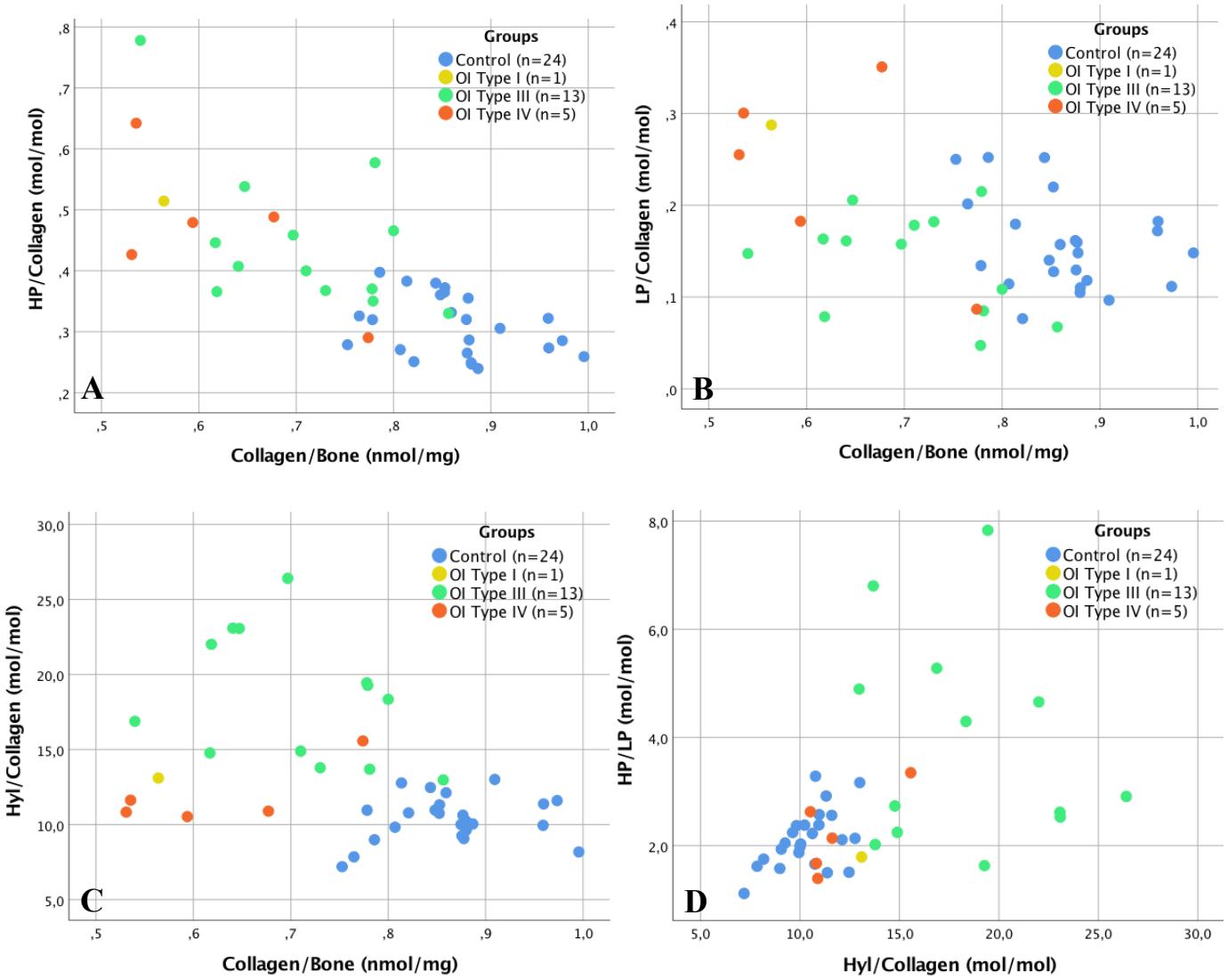

Figure 7. *Scatterplots of different biochemical parameters. Colors of the data points indicate OI type. The amount of crosslinks HP **(A)** and LP **(B)** are plotted against the collagen level per mg bone (dry weight). Hydroxylation of collagen is visualized in **(C)**. HP/LP crosslink ratios are plotted against Hyl levels in **(D)**.*

Linear regression is performed to check if increased hydroxylation might be a predictor for increased HP levels and HP/LP ratios. Regression was significant between Hyl and HP (R^2 = 0.168, F = 8.285, p = 0.006) and between Hyl and HP/LP (R^2 = 0.201, F = 10.332, p = 0.003). β-coefficients of the slope are provided in **Appendix G**.

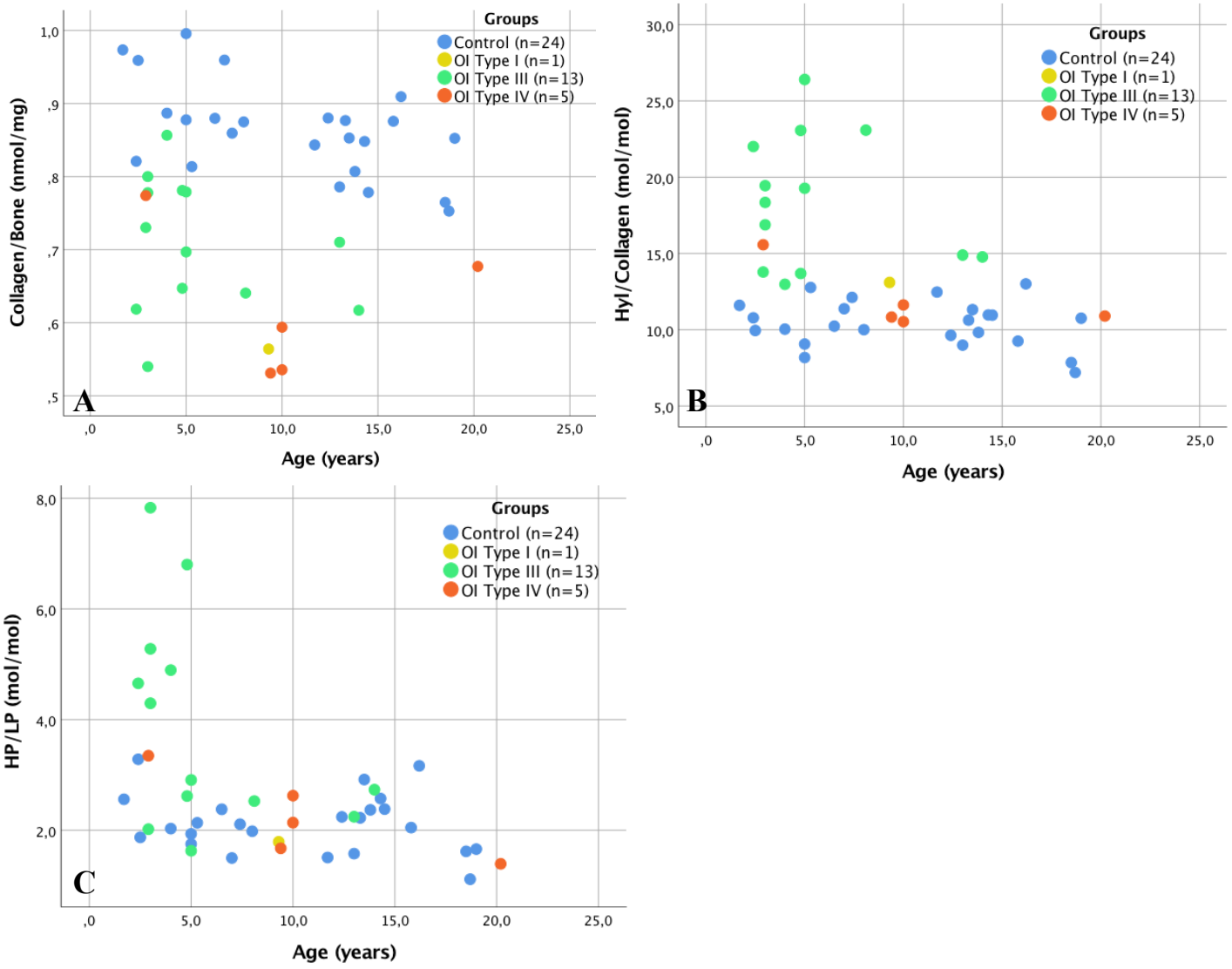

Figure 8. *Scatterplots of biochemical parameters plotted against the age of the patient during surgery. Collagen content per dry weight bone* ***(A)****, the lysyl hydroxylation* ***(B)*** *and the HP/LP crosslink ratio* ***(C)****. Colors of the data points indicate OI type.*

3.2 Bone density

Cortical bone samples are analyzed with micro-computed tomography. A calibration curve is derived from five HA phantoms with different densities in every measurement. All curves had $R^2 > 0.999$ and had similar linear relationship like y = 368.46x + 1039.7. Values for vBMD and vTMD are depicted in **Figure 9**. µCT images are analyzed and six OI bone samples had similar appearance as woven bone. This type of bone is characterized by a disorganized extracellular matrix, is mechanically weak and is a sign of fracture repair. Samples with such appearance are labelled with [1] in the plots. Means ± SD are stated in **Table 1**. Examples of µCT images of control, OI woven and OI non-woven are depicted in **Appendix H**.

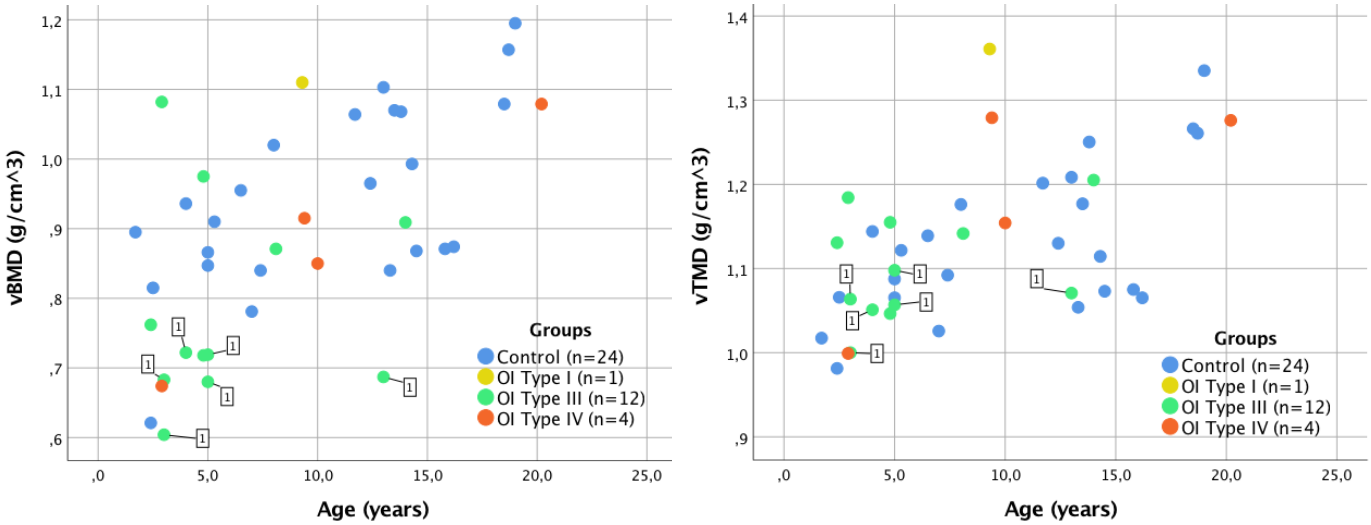

Figure 9. *Scatterplots of the vBMD **(Left)** and the vTMD **(Right)** plotted against the age of the patient during surgery. Six data points are labelled with [1], which indicates that bone samples are identified as woven by µCT images. Colors of the data points indicate OI type.*

	vBMD (g/cm^3)	vTMD (g/cm^3)
Control (n = 24)	0.94 ± 0.13	1.13 ± 0.09
OI, all (n=17)	0.83 ± 0.16	1.13 ± 0.10
OI, non-woven (n = 11)	0.90 ± 0.15	1.18 ± 0.10
OI, woven (n=6)	0.68 ± 0.04	1.06 ± 0.03

Table 1. *Values for vBMD and vTMD for control and OI samples. As the OI group contained some samples from woven bone, OI samples are categorized. Results are shown as mean ± SD.*

Individual values vBMD and vTMD are stated in **Appendix H**. The mean of the vTMD in the control and OI group was, based on histograms, normally distributed. According to Student's t-test, there were no significant differences observed in vTMD (t = -0.113, p = 0.993) between the controls and OI. vBMD is significantly higher in controls compared to OI (U = 124, p = 0.034). OI non-woven bone had significantly higher vBMD (U = 7.0, p = 0.009) and vTMD (U = 11.0, p = 0.027) values than OI samples from woven bone. Correlations between vBMD or vTMD and age are tested with Spearman's correlation coefficient ρ. In controls, vBMD (ρ = 0.581, p =0.003) and vTMD (ρ = 0.520, p = 0.009) were both significantly correlated with age. The vTMD (ρ = 0.548, p = 0.023) was correlated with age in OI bone tissue, but vBMD was not significantly correlated to age (ρ = 0.365, p = 0.150). No differences in either vBMD and vTMD are observed between type III and IV.

In addition, the tissue mineral density distribution is derived from the µCT images. A histogram is made from voxels with densities between 0.85 g/cm^3 and 1.7 g/cm^3. Every bin is divided by the total amount of voxels within that range to compensate for different bone sizes. The mean and standard deviation of every voxel density is calculated of all samples in the control or OI group. This distribution is shown in **Figure 10**. The red line indicates the mean of control bone samples and the shaded area is ± one standard deviation. OI samples are visualized in the same way in blue. Distributions of OI woven and non-woven bone are depicted in **Figure 11**.

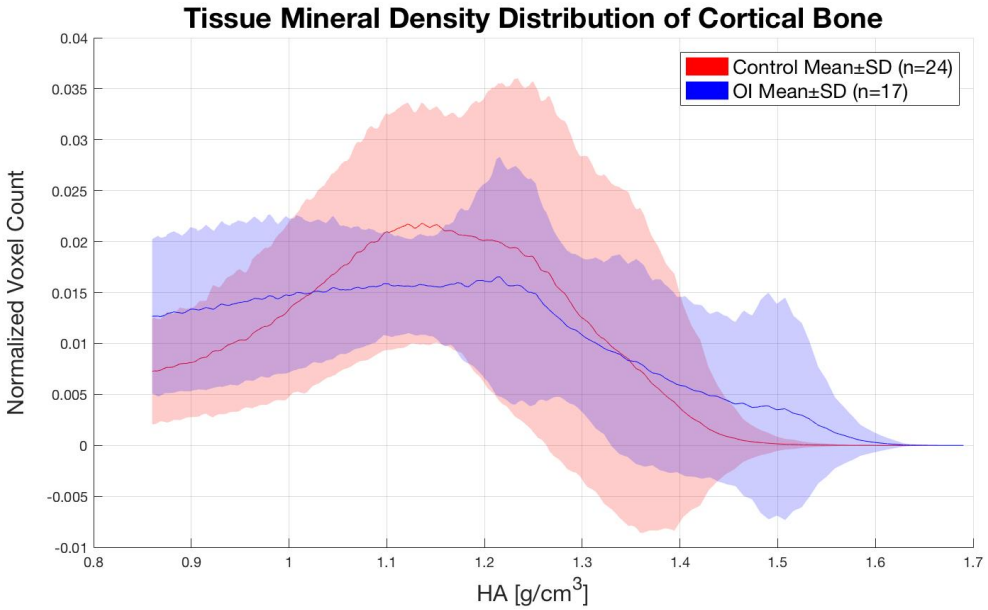

Figure 10. *Density distribution of cortical bone samples. In every sample, the frequency of each voxel density is counted and normalized over the total amount of measured voxels. The mean of all individual samples for each density is shown in this diagram. The red line represents the average voxel density in control bones, and the blue line is the mean of the OI samples. Red or blue shading around the line shows 1 SD above and below the mean.*

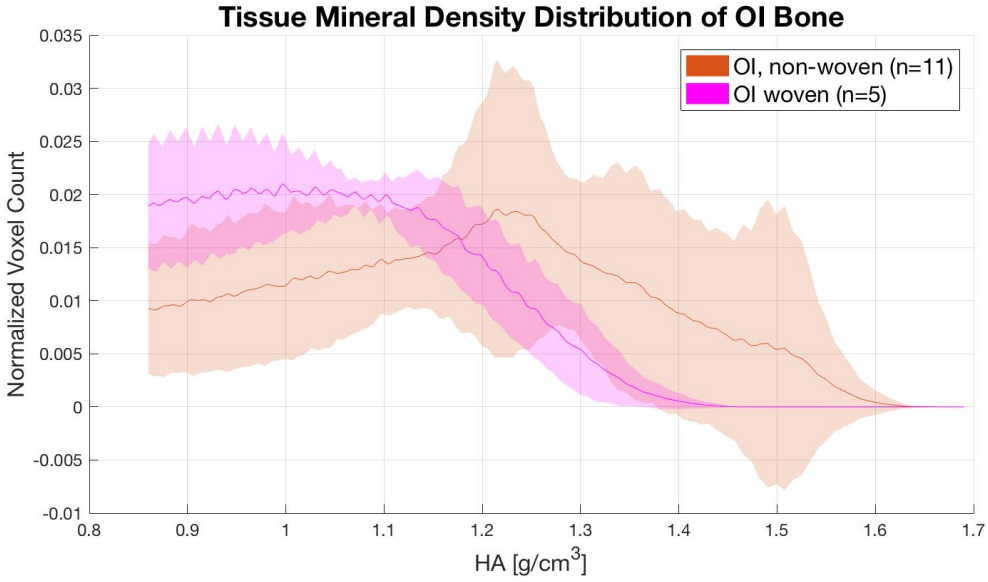

Figure 11. *Density distribution of cortical OI samples. In every sample, the frequency of each voxel density is counted and normalized over the total amount of measured voxels. The mean of all individual samples for each density is shown in this diagram. The pink line represents the average voxel density in woven-like OI bones. The brown line is the mean of the non-woven OI samples. Pink or brown shading around the line show 1 SD above and below the mean. Woven bone has lower mineralized areas, while non-woven OI samples tend to be hypermineralized.*

3.3 Mechanical properties

Young's modulus and hardness were obtained by indentation experiments. A piece of short fiber filled epoxy (Sawbones, Vashon Island, WA, USA) was used to test the protocol. Young's modulus and hardness were determined to be 80.1 MPa and 31.8 MPa, respectively. **Figure 12** shows a load-time curve and the corresponding load-displacement curve from one single measurement. The red line in the load-displacement curve shows the tangent which is used to determine the elastic unloading stiffness *S*.

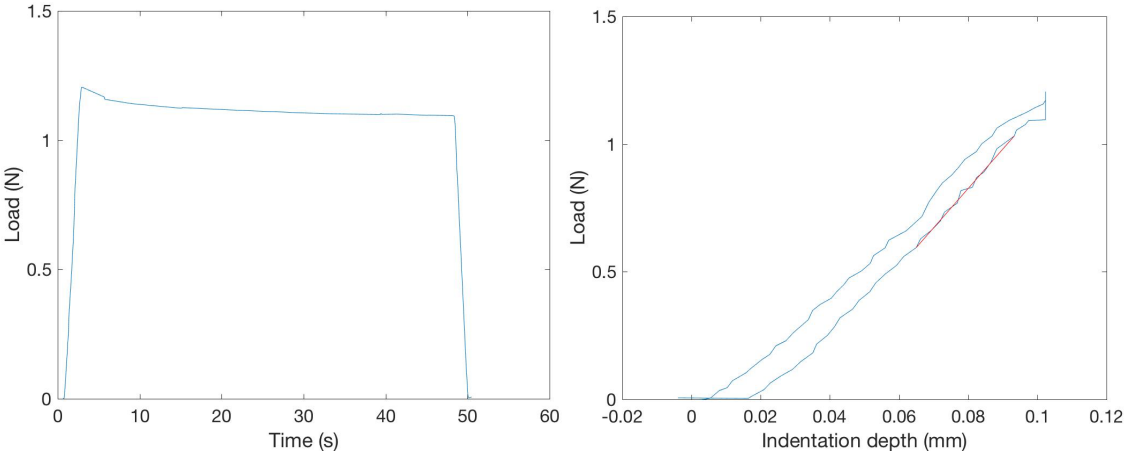

Figure 12. *Typical plots from indentation experiments with displacement control. Indentation is performed with a rate of 0.05mm/s to indentation depth of 0.1mm. The indenter head holds for 45s before it pulls back to its starting point with equal displacement rate.* ***(Left)*** *During this procedure, the load is measured as a function of time. Stress relaxation occurs after loading.* ***(Right)*** *The load-displacement curve of the same measurement is shown. The red line is the tangent of the first part during unloading and is used to determine the Young's modulus.*

Figure 13 (A, B) depicts separate sample measurements in mean ± SD error bars. For further analysis, woven and non-woven samples are depicted in different colors. Regarding hardness, histograms show that the means of control samples and OI samples are normally distributed. Student's t-test showed no significant differences in hardness between controls (M = 12.8, SD = 3.3) and OI samples (M = 12.2, SD = 4.5). **Table 2** shows values for Young's moduli and hardness in median (IQR) for comparison with Mann-Whitney U-test. No significant difference in Young's modulus between control bone and non-woven OI bones ($U = 78.0$, $p = 0.435$) are observed. Both mechanical properties were similar in woven and non-woven OI.

	Young's Modulus (MPa)	**Hardness (MPa)**
Control (n=19)	44.8 (41.3 – 45.8)	12.7 (10.5 - 15.1)
OI, all (n=16)	41.5 (38.6 - 46.2)	12.6 (8.8 -15.1)
OI, non-woven (n=10)	40.7 (39.4 - 46.5)	12.6(9.7 - 15.8)
OI, woven (n=6)	42.6 (31.1 - 46.2)	12.5(5.6 - 15.4)

Table 2. *Values for Young's modulus and hardness for control and OI samples. As the OI group contained some samples from woven bone, OI samples are categorized. Results are shown as median (IQR)*

Young's moduli and hardness of each sample are categorized by OI type in **Figure 13 (C, D)**. No significant differences between controls and OI groups are observed. **Figure 13 (E, F)** shows how the mechanical properties are distributed over age. No significant correlations are found between Young's modulus and age and hardness and age, in control or OI bones samples.

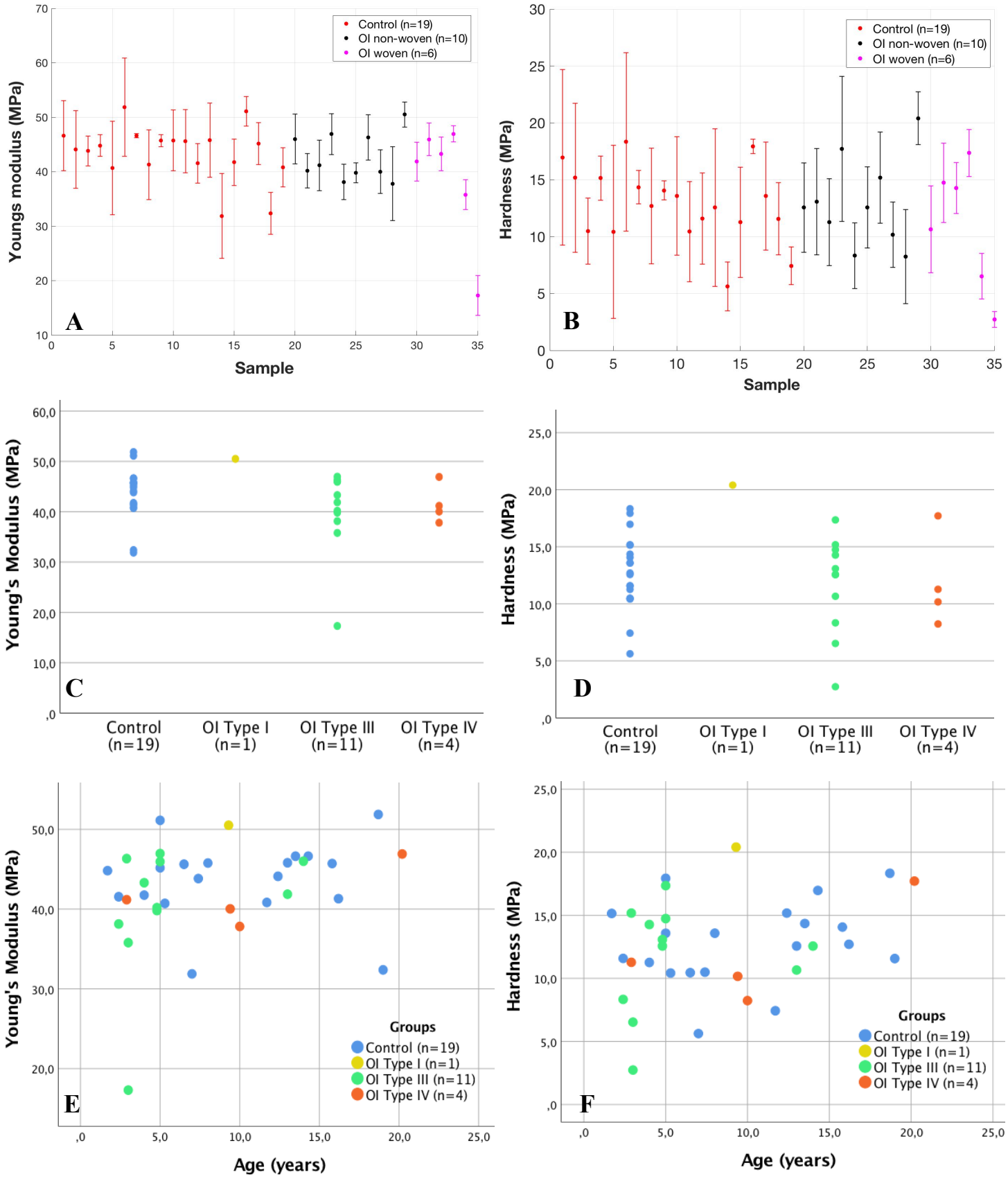

Figure 13. *Young's modulus and hardness of cortical bone obtained by indentation.* ***(A, B)*** *Error bars showing the mean and standard deviation of each individual measurement. Distinction is made between control, OI non-woven bone and OI woven bone.* ***(C, D)*** *Average Young's modulus and hardness of each sample divided in control and OI groups.* ***(E, F)*** *Average Young's modulus and hardness of each sample plotted against age. Colors of the data point indicate OI type.*

3.4 Correlations between parameters

Relationships between biochemical parameters, mechanical properties and density are investigated with Spearman's correlation efficient ρ. Correlations for control bone are shown in **Table 3**, whereas **Table 4** contains correlations in OI bones. Exact significance levels are stated in **Appendix I**. Significant correlations are plotted in **Appendix J** for controls and in **Appendix K** for OI samples

Control	*vBMD*	*vTMD*	*Hardness*	*Young's modulus*
vBMD		,901**	,212	,288
vTMD	,901**		-,019	,193
Age	,581**	,520**	,234	,166
Collagen/Bone	-,532**	-,561**	-,005	-,193
Hyl/Collagen	-,253	-,356	-,509*	-,621**
HP/LP ratio	-,236	-,415*	,161	,012
(HP+LP)/Collagen	,436*	,446*	-,098	,044
HP/Collagen	,322	,277	-,116	,009
LP/Collagen	,324	,440*	-,188	,007

Table 3. *Correlations between biochemical parameters, age, density and mechanical properties in control bone. Values are Spearman's correlation coefficient ρ. *. Correlation is significant at the 0.05 level (2-tailed), **. Correlation is significant at the 0.01 level (2-tailed)*

OI	*vBMD*	*vTMD*	*Hardness*	*Young's modulus*
vBMD		,887**	,491	,444
vTMD	,887**		,362	,447
Age	,365	,548*	,254	,378
Collagen/Bone	-,314	-,551*	,215	,112
Hyl/Collagen	-,569*	-,534*	-,085	-,118
HP/LP ratio	-,436	-,451	-,459	-,503*
(HP+LP)/Collagen	,275	,451	,068	-,026
HP/Collagen	,179	,294	-,047	-,197
LP/Collagen	,463	,525*	,382	,374

Table 4. *Correlations between biochemical parameters, age, density and mechanical properties in OI bone. Values are Spearman's correlation coefficient ρ. *. Correlation is significant at the 0.05 level (2-tailed), **. Correlation is significant at the 0.01 level (2-tailed)*

4. Discussion

Osteogenesis imperfecta is a group of genetic disorders characterized by skeletal dysplasia's and bone fragility. There is no cure and treatment is limited. Aim of this research is to gain more insight in the mechanisms behind this disease. In OI types I-IV, the disease originates from mutations in the COL1A1 or COL1A2 genes, which encode collagen type I α-chains. However, the pathophysiology of osteogenesis imperfecta is unclear. There are indications for disturbed collagen synthesis, although the exact working principle is not fully understood. Collagen molecules provide a framework for mineral deposition and are therefore responsible for the shape of the bone. In OI, structural parameters are inferior to normal healthy bone. The role of the collagen network to these parameters is uncertain. More research is needed for a better understanding of this disease, which is essential for the development of new treatments. In this study, different experiments are performed to examine the quality of the collagen molecules and to evaluate the mineralization in OI bone tissue. Mechanical indentation tests are carried out to determine if any relationships exist between post-translational overmodifications and mechanical properties in OI bone.

Bisphosphonates are administered to OI patients to increase vBMD and thereby the mechanical properties of the bone tissue. All OI patients in this study have a history of bisphosphonate treatment before bone fragments were retrieved during surgery. As these drugs inhibit bone resorption by osteoclasts, it is unlikely that biochemical parameters are affected. Sample sizes of OI types in this research are not equally distributed and sizes for type I (n = 1) and type IV (n = 5) are rather small for proper statistical analysis. As OI type III (n = 13) is more severe than type I and IV, it is expected that patients with type III are more likely to need orthopedic surgery. Although control samples are collected from patients with a variety of skeletal dysplasias, the bone tissue is assumed to be similar as completely healthy bone. In a few cases, bone fragments were not eligible for all the different experiments and data is missing.

HPLC is performed to examine the hydroxylation of proline and lysine in collagen molecules. Hydroxylated proline is an amino acid, specific for collagen and is therefore used to estimate collagen content in lyophilized bone, assuming 300 residues per collagen molecule. The collagen content per dry weight bone was significantly lower in OI samples versus controls ($U = 35$, $p < 0.001$). If the amount of collagen per mg bone is decreased, more bone mineral should be present. This is in agreement with a higher mineral-to-matrix ratio, as observed with Raman spectroscopy (Imbert et al., 2014) and substantiates indirectly the hypothesis of hypermineralization in OI.

It should be noted that all OI patients in this study received at least one bisphosphonate treatment. Lacking untreated OI patients, we are not able to verify that lower collagen content per mg lyophilized bone in OI is specific for this disease or an effect of drug treatment. Furthermore, weight of other proteins in bone tissue such as proteoglycans are neglected and no distinction is made between collagen type occurring in bone, such as type III.

Hyl residues in collagen are substrates for intermolecular crosslinking, which is essential in fibril formation. Overhydroxylation of lysine in OI is observed in dermis tissue (Petrovic and Miller, 1984) and cell cultures of skin fibroblasts (Kirsch et al., 1987; Lehmann et al., 1995). However, the extent of lysyl hydroxylation is tissue dependent (Yamauchi and Sricholpech, 2012) and only papers with results obtained from bone research, are used for comparison. Kirsch et al. showed that the lysyl hydroxylation in lethal OI type II was significantly increased compared to fetal newborns. Hyl levels in other OI types were similar

to controls. In this study however, the amount of Hyl residues per collagen molecule ($U = 35$, $p < 0.001$) was significantly increased in OI. This difference might occur due to endochondral ossification in the newborn control group of Kirsch. A different study used age-matched controls for comparison and found lysine overhydroxylation: 23.9 ± 5.2 Hyl/triple helix in OI (all types combined) versus 13.5 ± 2.4 Hyl/triple helix in control bone (Bank et al., 2000). Besides acid hydrolyzation, Bank et al. performed pepsin digestion to cleave collagen molecules in smaller peptides. Only hydrolyzation was performed in our study. This might indicate that pepsin digestion is essential to fully break down collagen into individual amino acid and explains our lower values: 16.37 ± 4.73 in OI versus 10.37 ± 1.50 Hyl/collagen in controls (means ± SD are shown in **Appendix G**).

Increased lysyl hydroxylation provides more Hyl residues to form HP crosslinks. HP and HP/LP ratio were indeed increased in OI compared to controls. To be more specific, Hyl residues and HP crosslinks were both more abundant in OI type III compared to type IV and compared to controls. HP/LP ratio was higher, although not significantly, in OI type III vs. type IV. Only one type I sample was at our disposal, which had similar Hyl/collagen and HP/LP values as controls. Individual crosslink values appeared to be higher. Although biochemical parameters are more modified in the severe type III, distinction between controls and OI type I and IV is not evident. Bank et al. did not found a correlation between phenotypic severity and crosslinking either.

The overhydroxylation of lysine influences is also related to glycosylation: the attachment of carbohydrates to the collagen α-chains during triple helix formation. All excess hydroxylysine residues were glycosylated in a patient with OI type II (Kirsch et al., 1981) Overglycosylation from fibroblast cultures is also found by others (Trelstad et al., 1977; Steinmann et al., 1984; Brinckmann et al., 1999). A relationship between overglycosylation of collagen type I and fibril diameter is observed several times (Grant et al., 1969; Steinmann et al., 1984; Notbohm et al., 1999). (Notbohm et al., 1999) performed *in vitro* measurements on type II collagen and concluded that collagen molecules with high Hyl levels are more glycosylated and form thin fibrils. Low Hyl levels generate fibrils with a larger diameter. Although the glycosylation is not measured in this study, we provide evidence that OI type III has more Hyl residues than controls and type IV. Because of glycosylation, it is plausible that collagen fibrils are thinner in OI type III compared to less severe types.

Two parameters regarding bone quantity are examined in this research. The vBMD is the average density of all voxels in a certain volume, whereas non-bone voxels are excluded in vTMD. For that reason, lower values for vBMD were observed in this study. This is expected due to the porous bone tissue observed in OI (Jameson, 2014; Imbert et al., 2015; Albert et al., 2017; Blouin et al., 2017). It should be emphasized that all patients received bone enhancing bisphosphonate treatments, which influences the absolute values for vBMD and vTMD. Furthermore, our μCT data is restricted by a limited resolution of the μCT (30μm), which is too low to detect osteocyte lacunae (1 - 10 μm) and other small pores. Partial volume effects will be more pronounced at the boundaries between pore and bone tissue. For this reason, pore size and shape is not further elucidated in present study.

Other studies performed similar μCT measurements with resolution up to 0.65 μm on OI and control bone (Imbert et al., 2015; Albert et al., 2017). OI patients in both studies were treated with bisphosphonates. Nevertheless, vBMD was lower in OI bone samples and absolute values are consistent with our results. In this study, vTMD was comparable between controls and OI. Imbert reported higher vTMD in OI, while Albert found similar values between the groups. This difference might occur due to the small sample sizes (n = 6-8). Positive correlations between vTMD and age are found in this study, which could explain

different reported values for vTMD. In present study, vTMD was not related to severity. However, the highest value originates from all measured samples originates from OI type I. The vBMD was also one of the highest observed values. Although only one single type I sample was measured, it is an interesting observation.

Six cases of woven-like bone are observed, which are all collected from patients with OI type III. vBMD and vTMD were significantly lower than non-woven OI bone. It is unclear if this structure is characteristic for severe OI or it is part of actual tissue repair. Some patients underwent surgery because of the bone fractures. If bone fragments are removed from the fracture site, the tissue consists of irregular shaped woven bone with lower density and weak mechanical properties.

Figure 10 shows the tissue mineral density distribution. This is frequently measured in literature with electron microscopy and is based on interactions with actual calcium atoms. Although the resolution of the µCT is not comparable with the high-quality images of electron microscopy, it still provides the same information. Generally, the distribution in OI is shifted to the right compared to control bones, indicating hypermineralization. This is observed in all OI types (Weber et al., 2006; Roschger et al., 2008; Fratzl-Zelman et al., 2014). For our controls, a peak is distinguished around 1.15 g/cm^3. No clear peak could be identified for OI bone, which means that OI bone is more heterogeneous. Low and high mineralization densities are more frequently detected in OI. The woven-like bone samples are the main cause for the increase in low mineralized bone areas (**Figure 11)**. The other OI samples contribute to the hypermineralized areas.

Mechanical properties of bone tissue obtained by indentation experiments do not show significant differences between OI and control bones. This is an unexpected finding, especially as OI is known as 'brittle bone disease'. At macroscale, compression experiments (Imbert et al., 2015) and three-point bending tests (Albert et al., 2017) showed drastically decreased Young's moduli and hardness in OI. Patients in these studies received bisphosphonates prior to bone fragment collection, which makes it unlikely that this treatment is the main cause of equal mechanical properties in our study population. Nano-indentation is performed in previous studies to characterize the tissue at nano-scale. Young's modulus and hardness were higher in OI than in controls, while values were equal after bisphosphonate treatment (Weber et al., 2006). Other studies observed similar mechanical properties in OI and controls (Fan et al., 2006; Z. Fan et al., 2007; Z. F. Fan et al., 2007). However, the indenter used in this study had a spherical tip with radius 0.25 mm, which measures mechanical properties on a different scale.

In the present study, the absolute values of the mechanical properties are not in the expected range. A composite obtained from Sawbones with similar mechanical properties as cortical bone is used as reference material. Young's modulus was determined at 80.1 MPa, while the manufacturer dictates a compressive modulus of 16.7 GPa. This indicates that indentation at this level measures different material properties than macroscale compression experiments. One study showed that indentation experiments in bone tissue do not reliably predict elastic moduli determined by compression (Boughton et al., 2018). However, a mean elastic indentation modulus of 4.42 GPa was observed with a spherical indenter (r = 0.75 mm) Relatively low mechanical properties in human bone measured by indentation experiments are observed previously. One study found Young's moduli of 119 – 234 MPa in human cadaver glenoids, using a flat cylindrical indenter (r = 1.25 mm) (Mimar et al., 2008). A Young's modulus of 325 MPa was measured during patellar indentations with a spherical tip**,** 1 mm in radius (Kerrigan et al., 2014). However, the latter used a Hertzian contact model for computations. Still, these values are clearly higher than our observed values.

Measurements from the indentation experiments in each sample show a high variation (**Figure 13 A, B**). This might indicate a very heterogeneous material. An inappropriate combination of indenter size and surface roughness could supply a second explanation. The first step of the indentation measurement is surface detection. The indenter is directed slowly towards the surface until an increase in load is detected. Bone tissue has a rough surface and it is unclear if the indenter hits the surface perpendicular or in a certain angle. If the indenter is too small, it slides over the surface instead of indenting the surface. A second scenario occurs when the indenter is slightly larger than the surface roughness. The contact area of the tip covers a gap during indentation, causing the contact area to be overestimated. Both cases lead to values lower than expected. Nevertheless, our composite phantom does not have such surface roughness and is assumed to be sufficiently smooth. This might indicate that different mechanical properties of the material are measured and that OI bone and control bone have similar properties at this scale. To find relationships between altered biochemical parameters and the fragile OI bone observed in patients, follow up studies should scale up the experiment with larger indenter tips to cover more bone material or perform other mechanical experiments such as compression or three-point bending experiments.

The mechanical results obtained in this study should be verified with additional measurements. First of all, the protocol needs extensive testing with different materials with known properties to prepare a calibration curve. In this study, the indenter head was damaged during autoclaving and no additional measurements are performed.

vBMD is known to increase with age in children and adolescents until peak mass is reached. In puberty, age dependency is higher (Boot et al., 1997). In this study, a significant relationship between age and vBMD is found. However, this was not observed in OI. We hypothesize that OI bone contains more primary mineralization sites due to more frequent (micro)fractures. This is bone tissue with low density and it takes months until mineral is fully incorporated in the matrix (Rauch and Schoenau, 2001).

The main components of bone tissue are collagen fibers embedded in mineral particles. In general, if the amount of collagen per mg dry bone increases, mineral mass per mg dry bone should be decreased. This negative relationship was evident in control bone.

Collagen density was significantly correlated to vBMD and vTMD. In OI, the amount of collagen was significant related to vTMD. Elevated intracortical porosity is a characteristic for OI and contributes to the vBMD. Therefore, a non-significant relation between vBMD and collagen density was expected.

Hyl residues were correlated in a negative way with vBMD and vTMD. Significant relations are only observed in OI. This might be due to the overhydroxylation in OI bone tissue. Collagen molecules are overglycosylated during synthesis and these bulky carbohydrate side chains interfere with a correct collagen packing. Collagen fibers are less organized, which inhibits sufficient mineral deposition. This effect will be more pronounced in OI bone due to the significant increased amount of Hyl residues in OI collagen molecules.

An unexpected finding is the significant correlation between LP/collagen and vTMD, in both controls and OI. LP levels were similar in both groups, while HP was increased in OI. Both LP and vTMD are significantly related with age in OI. LP crosslinks require a Lys residue to interconnect collagen molecules. Overhydroxylation in OI might cause a deficit in Lys residues, while LP crosslinks are essential for correct stereospecific crosslinking and thereby correct mineral deposition. More research is necessary to determine if LP is related to increased vTMD in this way.

As no significant difference occur between the control and OI group with respect to mechanical properties, hardly any significant correlations are observed with biochemical

parameters, vBMD or vTMD. However, Young's modulus is negatively correlated with HP/LP ratio in OI patients. This ratio determines the collagen packing and thereby the mechanical properties of the bone tissue. It is important to note that this correlation is only significant because of one single low value. If this value is assumed as an outlier, the relation is non-significant. The hardness of this value was also the lowest in all measured values, but was not convincingly an outlier. For this reason, this sample was not excluded. More mechanical experiments with a different indenter are necessary to determine if significant relationships exist between biochemical parameters and mechanical properties.

5. Conclusion

In this study, different experiments are performed to describe the quality, quantity and mechanical properties of OI bone tissue. Biochemical parameters obtained from liquid chromatography provide information about the quality of the collagen structure. The quantity of bone, in terms of vBMD and vTMD, is measured with μCT. Hardness and Young's moduli are derived from indentation experiments. In the introduction, we hypothesized that the structural and mechanical properties in bone samples from OI patients are related to post-translational modifications in collagen molecules. Our main findings are stated below.

Overhydroxylation of collagen is frequently observed in OI. We hypothesized that this leads to more HP crosslinks and increased HP/LP ratio's. That is actually what we observed in this study. Hyl levels were increased and regression analysis showed a significantly relation with increased HP and HP/LP values. Hyl levels were significantly higher in the severe OI type III compared with type I and IV.

In electron imaging, OI bone is found to be hypermineralized. This was indirectly observed in this study by a lower collagen content per mg of lyophilized bone. Six OI type III had a woven-like structure with lower vBMD and vTMD values than other OI samples. This likely reflects fracture repair and not a specific structural property of OI tissue itself. Average vTMD values were similar between OI and control bone. However, tissue mineral density distribution showed that OI bone was more heterogeneous. OI samples with woven-like structures had more areas with low density. Non-woven OI samples had more high density areas. The vBMD, the amount of bone tissue per volume accounting for porosity, was lower in OI.

Mechanical indentation with a spherical tip with radius of 0.25 mm showed no differences between controls and OI bone. No clear relationship was observed between altered crosslinking and mechanical behavior in OI bone tissue.

As a recommendation, indentation with a larger indenter tip is advised to cover more bone material and thereby likely creates less variable results. Mechanical properties are expected to be dramatically lower in OI. Therefore, different mechanical experiments should be considered to detect relationships with biochemical parameters. All OI patients in this study received bisphosphonate therapy prior to specimen collection. This affects the results obtained by μCT and indentation tests. In addition, follow-up studies should focus on glycosylation of collagen. These bulky carbohydrates might disturb the collagen packing, resulting in fibrils with smaller diameters. This effect could have impact on the mechanical properties of the bone tissue at organ level.

Bibliography

Albert, C., Jameson, J., Smith, P., & Harris, G. (2014). Reduced diaphyseal strength associated with high intracortical vascular porosity within long bones of children with osteogenesis imperfecta. *Bone, 66*, 121-130. doi:10.1016/j.bone.2014.05.022

Albert, C., Jameson, J., Tarima, S., Smith, P., & Harris, G. (2017). Macroscopic anisotropic bone material properties in children with severe osteogenesis imperfecta. *J Biomech, 64*, 103-111. doi:10.1016/j.jbiomech.2017.09.003

Albert, C., Jameson, J., Toth, J. M., Smith, P., & Harris, G. (2013). Bone properties by nanoindentation in mild and severe osteogenesis imperfecta. *Clin Biomech (Bristol, Avon), 28*(1), 110-116. doi:10.1016/j.clinbiomech.2012.10.003

Bank, R. A., Jansen, E. J., Beekman, B., & te Koppele, J. M. (1996). Amino acid analysis by reverse-phase high-performance liquid chromatography: improved derivatization and detection conditions with 9-fluorenylmethyl chloroformate. *Anal Biochem, 240*(2), 167-176. doi:10.1006/abio.1996.0346

Bank, R. A., Tekoppele, J. M., Janus, G. J., Wassen, M. H., Pruijs, H. E., Van der Sluijs, H. A., & Sakkers, R. J. (2000). Pyridinium cross-links in bone of patients with osteogenesis imperfecta: evidence of a normal intrafibrillar collagen packing. *J Bone Miner Res, 15*(7), 1330-1336. doi:10.1359/jbmr.2000.15.7.1330

Baron, R., Gertner, J. M., Lang, R., & Vignery, A. (1983). Increased Bone Turnover with Decreased Bone Formation by Osteoblasts in Children With Osteogenesis Imperfecta Tarda. *Pediatr Res, 17*(3), 204-207. doi:10.1203/00006450-198303000-00007

Bishop, N. (2016). Bone Material Properties in Osteogenesis Imperfecta. *J Bone Miner Res, 31*(4), 699-708. doi:10.1002/jbmr.2835

Blouin, S., Fratzl-Zelman, N., Glorieux, F. H., Roschger, P., Klaushofer, K., Marini, J. C., & Rauch, F. (2017). Hypermineralization and High Osteocyte Lacunar Density in Osteogenesis Imperfecta Type V Bone Indicate Exuberant Primary Bone Formation. *J Bone Miner Res, 32*(9), 1884-1892. doi:10.1002/jbmr.3180

Boot, A. M., de Ridder, M. A., Pols, H. A., Krenning, E. P., & de Muinck Keizer-Schrama, S. M. (1997). Bone mineral density in children and adolescents: relation to puberty, calcium intake, and physical activity. *J Clin Endocrinol Metab, 82*(1), 57-62. doi:10.1210/jcem.82.1.3665

Boudko, S. P., Engel, J., & Bachinger, H. P. (2012). The crucial role of trimerization domains in collagen folding. *Int J Biochem Cell Biol, 44*(1), 21-32. doi:10.1016/j.biocel.2011.09.009

Boughton, O. R., Ma, S., Zhao, S., Arnold, M., Lewis, A., Hansen, U., . . . Abel, R. L. (2018). Measuring bone stiffness using spherical indentation. *PLoS One, 13*(7), e0200475. doi:10.1371/journal.pone.0200475

Boyde, A., Travers, R., Glorieux, F. H., & Jones, S. J. (1999). The mineralization density of iliac crest bone from children with osteogenesis imperfecta. *Calcif Tissue Int, 64*(3), 185-190.

Brinckmann, J., Notbohm, H., Tronnier, M., Acil, Y., Fietzek, P. P., Schmeller, W., . . . Batge, B. (1999). Overhydroxylation of lysyl residues is the initial step for altered collagen cross-links and fibril architecture in fibrotic skin. *J Invest Dermatol, 113*(4), 617-621. doi:10.1046/j.1523-1747.1999.00735.x

Fan, Z., Smith, P. A., Eckstein, E. C., & Harris, G. F. (2006). Mechanical properties of OI type III bone tissue measured by nanoindentation. *J Biomed Mater Res A, 79*(1), 71-77. doi:10.1002/jbm.a.30713

Fan, Z., Smith, P. A., Harris, G. F., Rauch, F., & Bajorunaite, R. (2007). Comparison of nanoindentation measurements between osteogenesis imperfecta Type III and Type IV

and between different anatomic locations (femur/tibia versus iliac crest). *Connect Tissue Res, 48*(2), 70-75. doi:10.1080/03008200601090949

Fan, Z. F., Smith, P., Rauch, F., & Harris, G. F. (2007). Nanoindentation as a means for distinguishing clinical type of osteogenesis imperfecta. *Composites Part B: Engineering, 38*(3), 411-415. doi:10.1016/j.compositesb.2006.08.006

Fratzl-Zelman, N., Schmidt, I., Roschger, P., Glorieux, F. H., Klaushofer, K., Fratzl, P., . . . Wagermaier, W. (2014). Mineral particle size in children with osteogenesis imperfecta type I is not increased independently of specific collagen mutations. *Bone, 60*, 122-128. doi:10.1016/j.bone.2013.11.023

Grant, M. E., Freeman, I. L., Schofield, J. D., & Jackson, D. S. (1969). Variations in the carbohydrate content of human and bovine polymeric collagens from various tissues. *Biochim Biophys Acta, 177*(3), 682-685.

Gumustas, M., Kurbanoglu, S., Uslu, B., & Ozkan, S. A. (2013). UPLC versus HPLC on Drug Analysis: Advantageous, Applications and Their Validation Parameters. *Chromatographia, 76*(21-22), 1365-1427. doi:10.1007/s10337-013-2477-8

Imbert, L., Auregan, J. C., Pernelle, K., & Hoc, T. (2014). Mechanical and mineral properties of osteogenesis imperfecta human bones at the tissue level. *Bone, 65*, 18-24. doi:10.1016/j.bone.2014.04.030

Imbert, L., Auregan, J. C., Pernelle, K., & Hoc, T. (2015). Microstructure and compressive mechanical properties of cortical bone in children with osteogenesis imperfecta treated with bisphosphonates compared with healthy children. *J Mech Behav Biomed Mater, 46*, 261-270. doi:10.1016/j.jmbbm.2014.12.020

Jameson, J. R. (2014). *Characterization of Bone Material Properties and Microstructure in Osteogenesis Imperfecta/Brittle Bone Disease.* (Degree of Doctor of Philosophy), Marquette University, Milwaukee, Wisconsin. Retrieved from http://epublications.marquette.edu/dissertations_mu/413http://epublications.marquette.edu/dissertations_mu/413

Katti, K. S., Gu, C., & Katti, D. R. (2016). Anisotropic properties of human cortical bone with osteogenesis imperfecta. *Biomech Model Mechanobiol, 15*(1), 155-167. doi:10.1007/s10237-015-0727-4

Kerrigan, J. R., Sanchez-Molina, D., Neggers, J., Arregui-Dalmases, C., Velazquez-Ameijide, J., & Crandall, J. R. (2014). Indentation response of human patella with elastic modulus correlation to localized fractal dimension and bone mineral density. *J Mech Behav Biomed Mater, 33*, 99-108. doi:10.1016/j.jmbbm.2013.04.027

Kirsch, E., Krieg, T., Nerlich, A., Remberger, K., Meinecke, P., Kunze, D., & Muller, P. K. (1987). Compositional analysis of collagen from patients with diverse forms of osteogenesis imperfecta. *Calcif Tissue Int, 41*(1), 11-17.

Kirsch, E., Krieg, T., Remberger, K., Fendel, H., Bruckner, P., & Muller, P. K. (1981). Disorder of collagen metabolism in a patient with osteogenesis imperfecta (lethal type): increased degree of hydroxylation of lysine in collagen types I and III. *Eur J Clin Invest, 11*(1), 39-47.

Lehmann, H. W., Rimek, D., Bodo, M., Brenner, R. E., Vetter, U., Worsdorfer, O., . . . Muller, P. K. (1995). Hydroxylation of collagen type I: evidence that both lysyl and prolyl residues are overhydroxylated in osteogenesis imperfecta. *Eur J Clin Invest, 25*(5), 306-310.

Marini, J. C., Forlino, A., Bachinger, H. P., Bishop, N. J., Byers, P. H., Paepe, A., . . . Semler, O. (2017). Osteogenesis imperfecta. *Nat Rev Dis Primers, 3*, 17052. doi:10.1038/nrdp.2017.52

Mimar, R., Limb, D., & Hall, R. M. (2008). Evaluation of the mechanical and architectural properties of glenoid bone. *J Shoulder Elbow Surg, 17*(2), 336-341. doi:10.1016/j.jse.2007.07.024

Notbohm, H., Nokelainen, M., Myllyharju, J., Fietzek, P. P., Muller, P. K., & Kivirikko, K. I. (1999). Recombinant human type II collagens with low and high levels of hydroxylysine and its glycosylated forms show marked differences in fibrillogenesis in vitro. *Journal of Biological Chemistry, 274*(13), 8988-8992. doi:DOI 10.1074/jbc.274.13.8988

Oliver, W. C., & Pharr, G. M. (1992). An improved technique for determining hardness and elastic modulus using load and displacement sensing indentation experiments. *Journal of Materials Research, 7*(06), 1564-1583. doi:10.1557/jmr.1992.1564

Oliver, W. C., & Pharr, G. M. (2004). Measurement of hardness and elastic modulus by instrumented indentation: Advances in understanding and refinements to methodology. *J. Mater. Res.*(19). doi:10.1557/jmr.2004.19.1.3

Paschalis, E. P., Gamsjaeger, S., Fratzl-Zelman, N., Roschger, P., Masic, A., Brozek, W., . . . Fratzl, P. (2016). Evidence for a Role for Nanoporosity and Pyridinoline Content in Human Mild Osteogenesis Imperfecta. *J Bone Miner Res, 31*(5), 1050-1059. doi:10.1002/jbmr.2780

Petrovic, O. M., & Miller, E. J. (1984). An Unusual Pattern of Peptide-Bound Lysine Metabolism in Collagen from an Infant with Lethal Perinatal Osteogenesis Imperfecta. *Journal of Clinical Investigation, 73*(6), 1569-1575. doi:Doi 10.1172/Jci111363

Ramshaw, J. A., Shah, N. K., & Brodsky, B. (1998). Gly-X-Y tripeptide frequencies in collagen: a context for host-guest triple-helical peptides. *J Struct Biol, 122*(1-2), 86-91. doi:10.1006/jsbi.1998.3977

Rauch, F., & Schoenau, E. (2001). Changes in bone density during childhood and adolescence: an approach based on bone's biological organization. *J Bone Miner Res, 16*(4), 597-604. doi:10.1359/jbmr.2001.16.4.597

Rauch, F., Travers, R., Parfitt, A. M., & Glorieux, F. H. (2000). Static and dynamic bone histomorphometry in children with osteogenesis imperfecta. *Bone, 26*(6), 581-589.

Rijks, E. B., Bongers, B. C., Vlemmix, M. J., Boot, A. M., van Dijk, A. T., Sakkers, R. J., & van Brussel, M. (2015). Efficacy and Safety of Bisphosphonate Therapy in Children with Osteogenesis Imperfecta: A Systematic Review. *Horm Res Paediatr, 84*(1), 26-42. doi:10.1159/000381713

Roschger, P., Fratzl-Zelman, N., Misof, B. M., Glorieux, F. H., Klaushofer, K., & Rauch, F. (2008). Evidence that abnormal high bone mineralization in growing children with osteogenesis imperfecta is not associated with specific collagen mutations. *Calcif Tissue Int, 82*(4), 263-270. doi:10.1007/s00223-008-9113-x

Saito, M., & Marumo, K. (2015). Effects of Collagen Crosslinking on Bone Material Properties in Health and Disease. *Calcif Tissue Int, 97*(3), 242-261. doi:10.1007/s00223-015-9985-5

Sakkers, R., Kok, D., Engelbert, R., van Dongen, A., Jansen, M., Pruijs, H., . . . Uiterwaal, C. (2004). Skeletal effects and functional outcome with olpadronate in children with osteogenesis imperfecta: a 2-year randomised placebo-controlled study. *Lancet, 363*(9419), 1427-1431. doi:10.1016/S0140-6736(04)16101-1

Sillence, D. O., Senn, A., & Danks, D. M. (1979). Genetic heterogeneity in osteogenesis imperfecta. *J Med Genet, 16*(2), 101-116.

Sroga, G. E., & Vashishth, D. (2011). UPLC methodology for identification and quantitation of naturally fluorescent crosslinks in proteins: a study of bone collagen. *J Chromatogr B Analyt Technol Biomed Life Sci, 879*(5-6), 379-385. doi:10.1016/j.jchromb.2010.12.024

Ste-Marie, L. G., Charhon, S. A., Edouard, C., Chapuy, M. C., & Meunier, P. J. (1984). Iliac bone histomorphometry in adults and children with osteogenesis imperfecta. *J Clin Pathol, 37*(10), 1081-1089.

Steinmann, B., Rao, V. H., Vogel, A., Bruckner, P., Gitzelmann, R., & Byers, P. H. (1984). Cysteine in the triple-helical domain of one allelic product of the alpha 1(I) gene of type I collagen produces a lethal form of osteogenesis imperfecta. *J Biol Chem, 259*(17), 11129-11138.

Trelstad, R. L., Rubin, D., & Gross, J. (1977). Osteogenesis imperfecta congenita: evidence for a generalized molecular disorder of collagen. *Lab Invest, 36*(5), 501-508.

Vardakastani, V., Saletti, D., Skalli, W., Marry, P., Allain, J. M., & Adam, C. (2014). Increased intra-cortical porosity reduces bone stiffness and strength in pediatric patients with osteogenesis imperfecta. *Bone, 69*, 61-67. doi:10.1016/j.bone.2014.09.003

Weber, M., Roschger, P., Fratzl-Zelman, N., Schoberl, T., Rauch, F., Glorieux, F. H., . . . Klaushofer, K. (2006). Pamidronate does not adversely affect bone intrinsic material properties in children with osteogenesis imperfecta. *Bone, 39*(3), 616-622. doi:10.1016/j.bone.2006.02.071

Yamauchi, M., & Sricholpech, M. (2012). Lysine post-translational modifications of collagen. *Essays Biochem, 52*, 113-133. doi:10.1042/bse0520113

Abbreviations

OI	Osteogenesis imperfecta
HA	Hydroxyapatite
DXA/DEXA	Dual-energy x-ray absorptiometry
µCT	Micro computed tomography
vBMD	Volumetric bone mineral density
vTMD	Volumetric tissue mineral density
PTM	Post-translational modification
Gly	Glycine
Pro	Proline
Hyp	Hydroxyproline
Hyl	Hydroxylysine
Lys	Lysine
Gal	Galactose
Glc	Glucose
HP	Hydroxylysyl-pyridinoline
LP	Lysyl-pyridinoline
HPL	Hydroxylysyl-pyrroline
LPL	Lysyl-pyrroline
deH-LNL	Dehydro-lysinonorleucine
deH-HLNL	Dehydro-hydroxylysinorleucine
deH-DHLNL	Dehydro-dihydroxylysinorleucine
LH	Lysine hydroxylase
LOX	Lysyl-oxidase
LC	Liquid chromatography
HPLC	High-performance liquid chromatography
UPLC	Ultra-performance liquid chromatography
IS	Internal standard
FMOC	Fluorenylmethyloxycarbonylchloride
PBS	Phosphate buffered saline
IQR	Interquartile range
SD	Standard deviation

Appendices

Appendix A – Sample characteristics

CONTROL SAMPLES	SEX (M/F)	AGE (YEARS)	BONE
1	M	14.3	Femur
2	F	12.4	Femur
3	M	7.4	Fibula/Tibia
4	F	1.7	Fibula/Tibia
5	F	5.3	Fibula/Tibia
6	M	18.7	Femur
7	M	13.5	Femur
8	M	13.3	Fibula
9	M	11.7	Fibula
10	M	16.2	Femur
11	M	15.8	Femur
12	F	13.8	Femur
13	F	14.5	Fibula
14	M	2.5	Tibia
15	F	18.5	Femur/Fibula
16	M	8.0	Fibula/Tibia
17	F	6.5	Femur
18	F	2.4	Femur
19	F	13.0	Femur
20	F	7.0	Fibula
21	F	4.0	Femur
22	M	5.0	Fibula/Tibia
23	M	5.0	Fibula/Tibia
24	F	19.0	Femur/Fibula

OI SAMPLES	SEX (M/F)	AGE (YEARS)	BONE	OI TYPE
1	F	13.0	Femur	3
2	F	14.0	Tibia	3
3	F	8.1	Tibia	3
4	M	4.8	Femur/Tibia	3
5	F	2.9	Femur	4
6	Unknown	20.2	Tibia	4
7	F	2.4	Femur/Fibula/Tibia	3
8	F	5.0	Femur	3
9	F	4.8	Fibula/Tibia	3
10	M	4.0	Femur	3
11	F	2.9	Fibula/Tibia	3
12	F	9.4	Femur/Fibula/Tibia	4
13	M	9.3	Femur/Tibia	1
14	M	5.9	Femur	3
15	F	3.0	Femur	3
16	F	10.0	Fibula/Tibia	4
17	F	10.0	Fibula/Tibia	4
18	M	3.0	Femur/Fibula/Tibia	3
19	M	3.0	Femur/Fibula/Tibia	3

Appendix B – Sample preparations for chemical analysis

Before biochemical analysis, bone samples need to be cleaned thoroughly to remove other tissues. Dehydration is performed with lyophilization to obtain fully dry bone tissue composed of mineralized collagen. Then, the structure and macromolecules are completely partitioned in individual amino acids and other molecules by acid hydrolyzation to enable molecular separation by liquid chromatography.

Bone samples were washed with distilled water until the washing were free of blood. Then, the samples were defatted in Eppendorfs with a mixture of chloroform and methanol in a 2:1 (v/v) ratio for 30 minutes on a rollerbank. The liquid was removed and samples were placed in clean Eppendorfs in a -80°C freezer for 20 minutes. When the samples were fully frozen, they were lyophilized for 20-24 hours in a freeze dryer. The vessels were wrapped in aluminum foil to prevent bone tissue degeneration caused by light. A few tests were performed to ensure that 20 hours is sufficient to obtain fully dry bone specimen. Samples were weighted quickly after 20 hours of lyophilization, refrozen, and placed back in the freeze drier. After 4 hours, the mass was measured again and no difference in weight was observed. This means that all water is lyophilized and the samples are completely dry. Subsequently, bone samples were cut with a nibbler into pieces of 5 to 10 mg dry weight for crosslink measurements and 10-20 mg dry weight for amino acid analysis. All samples were hydrolyzed in 6M HCl (100µl/mg bone) in an oven at 110°C for 20-24 hours. Afterwards, evaporation of HCl succeeded by placing the Eppendorfs in a plate heater (40°C) with nitrogen blowing (2-2.5 bar) in each individual Eppendorf. For optimal evaporation speed, the nozzle is placed such that a small pit in the surface of the liquid is blown by the nitrogen flow. Lowering the nozzle during the process, accelerates the evaporation and it will take 4-7 hours (depending on the amount of HCl in the Eppendorfs) before the samples are completely dry and a yellow/brown residue is left at the bottom. Because of the rising HCl vapor, this procedure should be carried out under a fumehood. The residues are dissolved in internal standard solution for further analysis.

Appendix C – HPLC Protocol

HPLC analysis of FMOC derivatized amino acids

Reagents

- Boric acid (Sigma B0252)
- Pentane >95% (Interchema 601-006-00-1)
- Tri-sodiumcitrate-dihydrate (Merck 1.06448)
- Citric acid monohydrate (Sigma 251275)
- Tetramethylammonium chloride (Sigma T19526)
- Sodium azide (Sigma S2002)
- Phosphoric acid 85%wt (Acros Organics)
- Acetonitrile (Biosolve HPLC grade)
- Methanol absolute, HPLC (Biosolve, 136806)
- Acetone (Merck 100014)
- Sodiumhydroxide (Sigma S8045)
- 9-fluorenylmethyl chloroformate (Sigma 8.18203)
- 5 M NaOH: dissolve 6 g NaOH in 30 ml MilliQ water.
- 0.1 M borate buffer: dissolve 6.183 g boric acid in ± 900 ml MilliQ water. Bring the pH to 8.0 with 5 M NaOH; add Milli-Q water to 1000 ml. Store at 4 ºC; check before use the clarity of the solution (it should be clear).
- 0.1 M borate buffer: dissolve 6.183 g boric acid in ± 900 ml MilliQ water. Bring the pH to 8.0 with 5 M NaOH; add Milli-Q water to 1000 ml. Store at 4 ºC; check before use the clarity of the solution.
- 6 mM FMOC: dissolve in a stoppered glass tube 15 mg 9-fluorenylmethyl chloroformate in 10 ml acetone. Prepare freshly every day; avoid attraction of water from the air by closing the glass tube. With 10 ml about 40-45 samples can be derivatized.
- 25% (v/v) acetonitrile in 0.1 M borate buffer pH 8.0: Add 125 ml acetonitril to 375 ml 0.1 M borate buffer pH 8.0. Store at 4 ºC.

Preparation of Standards

- DL-5-Hydroxylysine hydrochloride (Sigma H0377)
- FMOC-L-Hydroxyproline ≥ 98%, HPLC (Sigma 47686)
- L-Lysine monohydrochloride ≥ 98% (Sigma L5626)
- L-homoarginine as internal standard (Sigma H1007)
- All samples & standards should contain 24µM homoarginine (=internal standard (IS) before derivatization with FMOC.
- 24 µM homoarginine internal standard solution: Dissolve 0.1348 g homoarginine in 50ml MQ (12mM). Take 0.4ml of 12mM to 200ml borate buffer pH 8.0 (24µM homoarginine)
- 60µM FMOC-Hyp: Dissolve 21.2 mg FMOC-Hyp in 1L of borate buffer pH 8.0
- 4.8mM Hyl: Dissolve 23.8mg Hyl in 25ml MQ
- 4.8mM Lys: Dissolve 21.9mg Lys in 25ml MQ
- 12µM Lys, 12µM Hyl, 60uM Hyp solution: add 0.5ml of 4.8mM Hyl and 0.5ml of 4.8mM Lys to 199 ml Hyp buffer.
- 12µM Lys, 12µM Hyl, 60uM Hyp, 24µM homoarginine solution: add 0.4ml of 24µM homoarginine to the 12µM Lys, 12µM Hyl, 60uM Hyp solution

Different concentrations of the external calibrators for a calibration curve

Concentration of Hyp/Hyl/Lys/Homo [µM]	Amount of buffer with Hyp/Hyl/Lys/Homo [ml]	Amount of buffer with only homoarginine [ml]	Dilution factor
60/12/12/24	1	0	1
45/9/9/24	0.75	0.25	1.33
30/6/6/24	0.5	0.5	2
15/3/3/24	0.25	0.75	4
6/1.2/1.2/24	0.1	0.9	10
3/0.6/0.6/24	0.05	0.95	20

In each sample and standard 400pmol of homoarginine was injected with a retention time of 9.1 minutes. Excess FMOC from the derivatization step was clearly visible as a high peak at RT = 14.3 min.

	RT (min)	Range of curve	R^2 of curve
FMOC-Hydroxyproline (Hyp)	10.15	50-1000 pmol	0.99
Hydroxylysine (Hyl)	23.35	10-200 pmol	0.99
Lysine (Lys)	24.95	10-200 pmol	0.99

Preparation of samples

- Dissolve the dry residues in internal standard solution 50µl/mg IS solution. In most of the cases a brown precipitate is visible even after rigorous vortexing due to hydrolyzed sugars (e.g. derived from proteoglycans). Centrifuge the vortexed samples in an Eppendorf centrifuge for at least 2 minutes. Use the clear supernatant (that is usually yellow to brown, depending on the type and amount of tissue) for analysis. Material that is not used for amino acid or cross-link analsyis can be stored at -20 ºC for many years
- Samples are diluted 250x to lower the molarity of the amino acids: 96µl of IS solution is put into an Eppendorf and 4µl of clear supernatant is added. This solution was vortexed rigorously and 200µl is injected into an empty Eppendorf tube for derivatization.

Derivatisation of amino acids with FMOC

Protocol

- Add 200 µl sample (dissolved in 0.1 M borate buffer pH 8.0) or 200 µl amino acid standard pH 8.0 in a safe lock Eppendorf tube
- Add 200 µl 6 mM FMOC, vortex immediately, allow to stand at room temperature for at least 5 minutes. FMOC gives with amino acids a strong fluorescent signal; the FMOC reacts with both secondary and primary amino acids. A 75-fold excess of FMOC is present
- Add 600 µl pentane, vortex rigorously (extraction step!), allow to stand at room temperature for at least 1 minute (in order to allow phase separation), and remove the upper layer (with this extraction step the hydrolysis product of FMOC with water (=FMOC-OH), the excess FMOC and the acetone is removed). Carry the extraction out in a fume hood. The phase separation is mostly near very clear.
- Repeat the extraction step
- Add to the remaining lower layer 400 µl 25% (v/v) acetonitrile in 0.1 M borate buffer pH 8.0 and vortex
- Add 150 µl of the mixture into HPLC inserts

HPLC analysis of FMOC derivatized amino acids

Apparatus:

- Waters 2795 Separations Module
- Column: TosoHaas TSKgel ODS-80-TM, 4.6 mm ID x 15 cm;
- Waters 2475 HPLC Multi Fluorescence detector (excitation 254 nm, emission 630 nm)
- Waters Empower 3 Chromatography Data software programme for data analysis

Machine settings:

- Analysis time: 0:40:00
- Injection volume: 50 µl
- Column temperature: 30°C
- Sample environment temperature: 20°C.
- Initial system pressure before sample injection (50µl) was 1790 psi with a steady pressure ripple between 15-20 psi.
- Flow rate of 1.4ml/min.
- The injection needle was washed after every injection with 10% methanol.
- After measurements, the column is washed and stored in 100% acetonitrile.

Chromatographic gradient conditions for HPLC analysis

Time (0.1 min)	**% eluent A**	**% eluent B**	**% eluent C**	**Flow µl/min.**
	citrate pH 2.85	**citrate pH 4.5**	**Acetonitrile**	
0	75		25	1400
115	60		40	1400
130	60		40	1400
131		64	36	1400
180		62	38	1400
250		30	70	1400
300		25	75	1400
320		25	75	1400
321	75		25	1400
400	75		25	1400

Preparation of eluents:

- *solution 1*
  8,56 g citric acid
  1.10 g tetramethylammonium chloride
  200 mg sodium azide
  Dissolve in 2000 ml Milli-Q water
- *solution 2*
  11.17 g tri-sodiumcitrate-dihydrate
  1.10 g tetramethylammonium chloride
  200 mg sodium azide
  Dissolve in 2000 ml Milli-Q water
- **Eluent A:** bring 1600 ml solution 1 to pH 2,85 with solution 2 (about 200 ml)
- **Eluent B:** bring 1600 ml solution 2 to pH 4.5 with phosphoric acid, add 400 ml methanol
- **Eluent C:** acetonitrile

Appendix D – UPLC Protocol

Protocol for cross-link analysis in bone samples

Reagents

- Acetonitrile, HPLC (Biosolve 012007)
- Acetone (Merck 100014)
- Heptafluorobutyric acid (HFBA) 99% GC (Sigma 77429)
- Pyridoxine hydrochloride ≥ 98%, HPLC (Sigma P9755)
- External calibrator for cross-link analysis (Quidel Corporation, Catalog Number 8004), stored at 2-8ºC. This standard contains 5.91µg/ml hydroxylysyl-pyridinoline (HP) and 3.08 µg/ml lysyl-pyridinoline (LP).

Preparation of Standards

- Stock solution pyridoxine (10 mM) (for the preparation of the internal standard solution): Dissolve 0.2056 g pyridoxine monohydrochloride in exactly 100 ml Milli-Q water. Store at -20 ºC in 10 ml tubes. Thawed samples should be vortexed rigorously before use.
- 10µM pyridoxine: dilute 200 µl stock solution pyridoxine to exactly 200 ml with Milli-Q water. Store the solution at -20 ºC; at 4 ºC it is stable for at least 1 month. Freshly thawed samples should be vortexed rigorously before use.
- 1% (v/v) HFBA in 10% (v/v) acetonitrile in 1µM pyridoxine (internal standard solution): 79 ml Milli-Q water + 1 ml HFBA + 10 ml acetonitrile + 10ml 10µM pyridoxine. Store at room temperature; prepare freshly every 2-3 weeks.
- External calibrator for cross-link analysis (Quidel Corporation, Catalog Number 8004), stored at 2-8ºC. This standard contains 5.91µg/ml pyridinoline (HP) and 3.08 µg/ml deoxypyridinoline (LP).

Preparation of external calibrators

- The external calibrator is diluted to different concentrations to generate a calibration curve. All calibrators are diluted in such a way that the composition is similar to the sample solution: 10% (v/v) acetonitrile, 10% (v/v) 10µM internal standard solution and 1% (v/v) HFBA.
- Stock solution for this dilution solution: 5ml acetonitrile + 5ml internal standard solution + 0.5ml HFBA. Prepare freshly every 2-3 weeks.
- The table below shows multiple compositions to prepare different calibrators:

Calibrator % (v/v)	External standard (µl)	MQ (µl)	Dilution-solution (µl)
0%	0	79	21
2.5%	2.5	76.5	21
5%	5	74	21
10%	10	69	21
15%	15	64	21
20%	20	59	21
30%	30	49	21

- The table below shows the molarity (µM) of the crosslinks HP and LP for the different calibrators and the amount of crosslinks (pmol) injected into the UPLC system by an injection volume of 5µl. All calibrators are fitted in a linear calibration curve with $R^2 \geq 0.99$

Calibrator % (v/v)	HP in standard [µM]	HP injected (pmol)	LP in standard [µM]	LP injected (pmol)
0%	0	0	0	0
2.5%	0.345	1.725	0.187	0.935
5%	0.690	3.45	0.373	1.865
10%	1.379	6.895	0.747	3.735
15%	2.069	10.345	1.120	5.6
20%	2.759	13.795	1.494	7.47
30%	4.138	20.69	2.240	11.2

Preparation of samples

- Dissolve the dry samples in 1% (v/v) HFBA, 10% (v/v) acetonitrile in 1µM IS solution to a volume of 1 ml. Samples can be stored at -80ºC until use.
- Before UPLC analysis, thawed samples should be vortexed rigorously and centrifuged for 5 minutes. Add 100µl of clear supernatant to the UPLC inserts.

UPLC analysis of the cross-links HP and LP

Apparatus:

- Waters ACQUITY UPLC M-Class System
- Precolumn: ACQUITY UPLC BEH C18 VanGuard Pre-column, 130Å, 1.7 µm, 2.1 mm X 5 mm
- Column: ACQUITY UPLC BEH C18 Column, 130Å, 1.7 µm, 2.1 mm X 50 mm

Preparation of eluents:

- Eluent A: 0.12% (v/v) HFBA in Milli-Q water
  0.60 ml HFBA + 500 ml Milli-Q water
- Eluent B: 1:1 (v/v) mixture of eluent A: acetonitrile
  150 ml of eluent A + 150 ml acetonitrile

UPLC Settings

- Column flow rate: 0.667 ml/min
- Column temperature of 50ºC and sample temperature of 20ºC
- Injection volume: 5µl
- Starting composition: 90% eluent A and 10% eluent B
- Analysis time: 5 min
- Gradient of eluent B rises from 10% to 20.5%
- Followed by 2 minutes of washing the column with the starting composition of 90% eluent A
- Fluorescence: excitation 297 nm and emission 395 nm (wavelengths for HP and LP)
- After the measurements, the column is washed and stored in 50% acetonitrile.

Appendix E – Matlab code for micro-CT data analysis

```
clear all
close all
clc

addpath(genpath(fullfile(pwd,'../Function/inpaint_nans.m')))
addpath(genpath(fullfile(pwd,'../Function/boundedline.m')))
addpath(genpath(fullfile(pwd,'../Function/catuneven.m')))
addpath(genpath(fullfile(pwd,'../Function/singlepatch.m')))
addpath(genpath(fullfile(pwd,'../Function/mean_plots.m')))

min_HA = 0.85;        %minium HA density in g/cm3
max_HA = 1.7;         %maximum HA density in g/cm3
xq =linspace(min_HA+0.01,max_HA-0.01,15000); % Create a range that enables
interpolation
filename = 'Density.xlsx';

 %% Control Samples: Femur - Tibia - Fibula
sheet = 'Controls';             % Select right data sheet
[num, txt]=xlsread(filename,sheet,'');
samp=length(txt);
loop = 0;
for i=1:2:(samp-1)
    loop = loop+1;
    % Retrieve hydroxyapatite (HA) density & amount of pixels from excel
    value=num([3:end],i)/1000;       % HA density in g/cm3
    count=num([3:end],i+1);         % Amount of pixels with that HA density
    oldmatrix=[value count];
    % Create matrix with predefined HA range
    newmatrix = oldmatrix;
    newmatrix= oldmatrix([value < max_HA & value > min_HA],:);
    % Calculate mean HA density for each sample
    sample_mean = sum(newmatrix(:,1).*newmatrix(:,2))/sum(newmatrix(:,2));
    % Calculate sum of all voxels in range
    area = sum(newmatrix(:,2));
    % Normalize every measurement by total amount of voxels
    normalized = newmatrix(:,2)/area;
    % Interpolate between measurements to obtain same amount of
    % measurements in range
    vq=interp1(newmatrix(:,1),normalized,xq);
    new(:,loop)=vq';
    % Store the means in a vector
    vector_sample_means(loop) = sample_mean;
end
% Calculate mean&SD of all means
control_Fem_Tib_Fib_mean = mean(vector_sample_means)
control_Fem_Tib_Fib_SD = std(vector_sample_means)
% Calculate mean&SD at every interpolated point of all control samples for
% plot
new(isnan(new))=0;
control_Fem_Tib_Fib_plotmean=mean(new,2);
control_Fem_Tib_Fib_plotstd =std(new,0,2);

%% Plots

tmdall=figure
boundedline(xq, [control_Fem_Tib_Fib_plotmean],
[control_Fem_Tib_Fib_plotstd],'red','alpha')
title('Tissue Mineral Density Distribution of Cortical Bone')
xlabel('HA [g/cm^3]')
ylabel('Normalized Voxel Count')
legend('Control Fem/Tib/Fib SD', 'Control mean (n=24)')
grid on
```

Appendix F – Matlab code for indentation data analysis

```
clear all
close all
clc

filename = 'Indentation.xlsx';

%% Properties
v_bone = 0.3;          %Poisson ratio of bone
v_indent = 0.3;        %Poisson ratio of indenter head (stainless steel)
E_indent = 200e9;      %Youngs modulus of indenter head (stainless steel)
r = 0.25e-3;           %Radius of indenter head: 0.25mm
h = 0.1e-3;            %Indention depth 0.1mm
B = 1;                 %Geometrical correction factor (beta = 1 for a sphere)
epsilon=0.75;          %Geometric constant (epsilon = 0.75 for a sphere)

i_up = 960;            % Index at end of stage hold
i_low = 972;           % Index at aprox 70% of unloading slope

%% OI
sheet = 'OI';
[num, txt]=xlsread(filename,sheet,'');
loop=0;
for i=1:3:length(txt)
    loop =loop+1;
    Load = num([2:1000],i+1);
    Disp = num([2:1000],i+2);
    Load_1 = Load(i_up);
    Load_2 = Load(i_low);
    Disp_1 = Disp(i_up);
    Disp_2 = Disp(i_low);
    Load_max=Load(940);                    % Maximum load before unloading
    S = (Load_1-Load_2)/((Disp_1-Disp_2)*1e-03);      % Unloading stiffness
    h_c = h-epsilon*Load_max/S;                       % Contact depth
    A_c = 2*pi*r*h_c;
    E_eff = 0.5*sqrt(pi)*S/sqrt(A_c);
    E = (1-(v_bone)^2)/((1/E_eff)-((1-(v_indent)^2)/E_indent));
    H = Load_max/A_c;
    E_OI(loop) = E;
    H_OI(loop) = H;
    OI(loop)=txt(1,i);
end

%% Calculate mean and std of every OI sample (3 measurements/sample)
count = 1;
for j = 1:3:length(E_OI)-2
    E_OI_meanvector(count) = mean(E_OI(j:j+2));
    E_OI_stdvector(count) = std(E_OI(j:j+2));
    H_OI_meanvector(count) = mean(H_OI(j:j+2));
    H_OI_stdvector(count) = std(H_OI(j:j+2));
    count = count+1;
end

% Sample 112 had just 2 suitable measurements
E_OI_meanvector(17) = mean(E_OI(49:50));
E_OI_stdvector(17) = std(E_OI(49:50));
H_OI_meanvector(17) = mean(H_OI(49:50));
H_OI_stdvector(17) = std(E_OI(49:50));
```

Appendix G – Supplementary biochemical results

Calibration data for HPLC & UPLC measurements:

Method	*Compound*	*Retention Time (min)*	*Curve equation*	R^2
HPLC	Homoarginine (IS)	9.1		
	Hyp	10.15	Y = 0.994+1.11*X	0.998
	Hyl	23.35	Y = 0.345+2.05*X	0.998
UPLC	Pyridoxine (IS)	1.05		
	HP	2.80	Y = -0.0336+0.541*X	0.997
	LP	3.28	Y = -0.011+0.317*X	0.995

Y = amount of compound in µM and X = area under the curve of the peak.

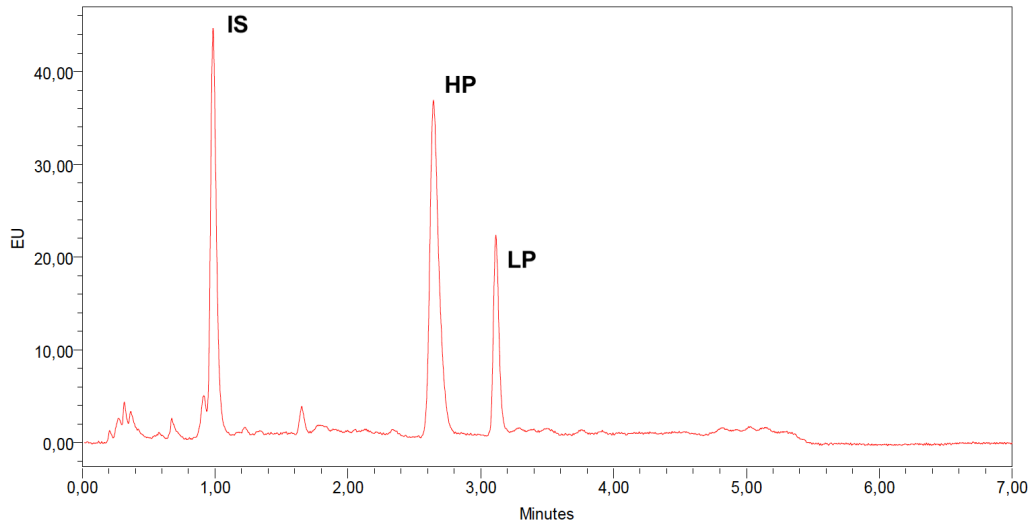

Figure 15. *Chromatogram from UPLC measurements. Showing the retention times of the internal standard (IS) and the crosslinks HP and LP.*

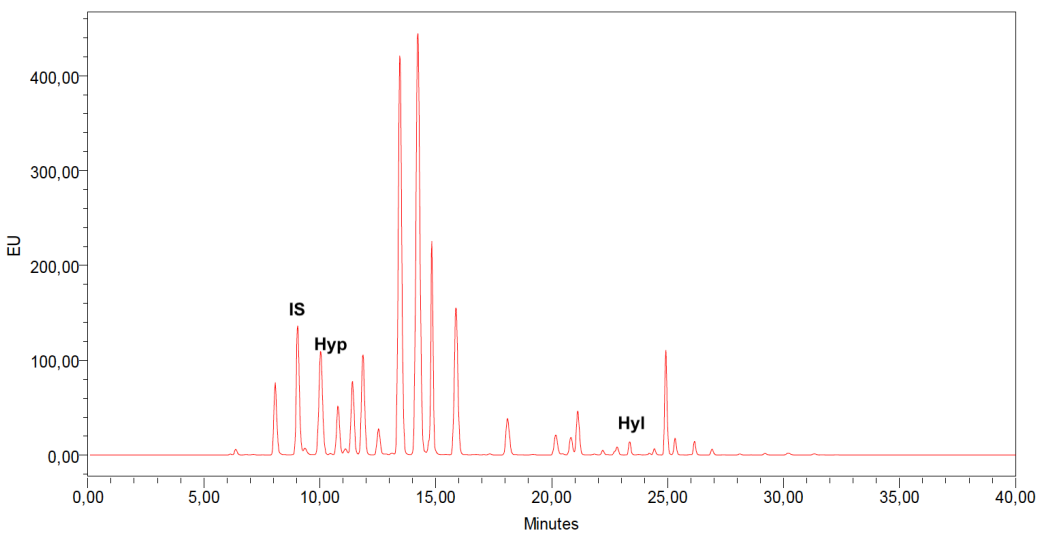

Figure 16. *Chromatogram from HPLC measurements. Showing the retention times of the internal standard (IS) and the amino acids Hyp and Hyl.*

	Control (n = 24)	OI (n = 19)	U	P value
Collagen/dry bone (nmol/mg)	0.87 (0.82-0.89)	0.68 (0.59-0.78)	25.0	**P < 0.001**
Hyl/collagen (mol/mol)	10.42 (9.3-11.36)	14.89 (12.98-19.44)	35.0	**P < 0.001**
HP/LP (mol/mol)	2.08 (1.68-2.38)	2.62 (2.01-4.66)	126.0	**P = 0.013**
HP/collagen (mol/mol)	0.31 (0.27-0.36)	0.45 (0.37-0.51)	40.0	**P < 0.001**
LP/collagen (mol/mol)	0.15 (0.12-0.18)	0.16 (0.09-0.22)	204.0	P = 0.557
(HP+LP)/collagen (mol/mol)	0.47 (0.40-0.52)	0.61 (0.55 – 0.74)	86.0	**P = 0.001**

Comparison between of biochemical parameters between control and OI. *Results are shown as median (IQR), Significant differences between control and OI bone samples are stated in bold.*

	Control (n = 24)	OI (n = 19)	OI I (n=1)	OI III (n=13)	OI IV (n=5)
Collagen/Bone (nmol/mg)	0.86 ± 0.06	0.68 ± 0.1	0.56	0.71 ± 0.09	0.62 ± 0.1
Hyl/Collagen (mol/mol)	10.37 ± 1.50	16.37 ± 4.73	13.10	18.35 ± 4.31	11.88 ± 2.10
HP/LP (mol/mol)	2.12 ± 0.53	3.34 ± 1.78	1.79	3.88 ± 1.93	2.23 ± 0.78
HP/Collagen (mol/mol)	0.31 ± 0.05	0.46 ± 0.12	0.51	0.45 ± 0.12	0.46 ± 0.13
LP/Collagen (mol/mol)	0.16 ± 0.05	0.17 ± 0.08	0.29	0.14 ± 0.05	0.24 ± 0.10
(HP+LP)/Collagen (mol/mol)	0.47 ± 0.09	0.63 ± 0.17	0.80	0.59 ± 0.14	0.70 ± 0.21

Results of liquid chromatography. *Results are categorized per OI type and shown as mean ± SD.*

Control+OI	*Indep. Var.*	*Dep. Var.*	R^2	*F (p)*	*β , constant (p)*	*β , coeff. (p)*
	Hyl	HP	0.168	8.285 (0.006)**	0.240 (<0.001)***	0.010 (0.006)**
	Hyl	HP/LP	0.201	10.332 (0.003)**	0.834 (0.171)	0.140 (0.003)**

Results of regression analysis.

****. Correlation is significant at the < 0.001 level (2-tailed).*

***. Correlation is significant at the 0.01 level (2-tailed).*

Spearman Correlations in Control Bone Samples

		Collagen/Bone	Hyl/Collagen	HP/LP ratio	HP/collagen	LP/Collagen	HP+LP/Collagen	Age
Collagen/Bone	Correlation Coefficient	1,000	,146	,097	-,428*	-,371	-,470*	-,537**
	Sig. (2-tailed)	.	,496	,651	,037	,074	,020	,007
Hyl/Collagen	Correlation Coefficient	,146	1,000	,451*	,329	-,189	,056	-,148
	Sig. (2-tailed)	,496	.	,027	,117	,377	,796	,491
HP/LP ratio	Correlation Coefficient	,097	,451*	1,000	-,163	-,844**	-,534**	-,105
	Sig. (2-tailed)	,651	,027	.	,445	,000	,007	,625
HP/Collagen	Correlation Coefficient	-,428*	,329	-,163	1,000	,636**	,885**	,293
	Sig. (2-tailed)	,037	,117	,445	.	,001	,000	,165
LP/Collagen	Correlation Coefficient	-,371	-,189	-,844**	,636**	1,000	,884**	,252
	Sig. (2-tailed)	,074	,377	,000	,001	.	,000	,235
HP+LP/Collagen	Correlation Coefficient	-,470*	,056	-,534**	,885**	,884**	1,000	,391
	Sig. (2-tailed)	,020	,796	,007	,000	,000	.	,059
Age	Correlation Coefficient	-,537**	-,148	-,105	,293	,252	,391	1,000
	Sig. (2-tailed)	,007	,491	,625	,165	,235	,059	.

*. Correlation is significant at the 0.05 level (2-tailed).

**. Correlation is significant at the 0.01 level (2-tailed).

Spearman Correlations in OI Bone Samples

		Collagen/bone	Hyl/Collagen	HP/LP ratio	HP/Collagen	LP/Collagen	HP+LP/Collagen	Age
Collagen/Bone	Correlation Coefficient	1,000	,267	,351	-,477*	-,544*	-,647**	-,415
	Sig. (2-tailed)	.	,270	,141	,039	,016	,003	,078
Hyl/Collagen	Correlation Coefficient	,267	1,000	,332	-,211	-,435	-,354	-,462*
	Sig. (2-tailed)	,270	.	,166	,387	,063	,137	,046
HP/LP ratio	Correlation Coefficient	,351	,332	1,000	-,026	-,912**	-,344	-,577**
	Sig. (2-tailed)	,141	,166	.	,915	,000	,149	,010
HP/Collagen	Correlation Coefficient	-,477*	-,211	-,026	1,000	,393	,918**	,366
	Sig. (2-tailed)	,039	,387	,915	.	,096	,000	,123
LP/Collagen	Correlation Coefficient	-,544*	-,435	-,912**	,393	1,000	,661**	,679**
	Sig. (2-tailed)	,016	,063	,000	,096	.	,002	,001
HP+LP/Collagen	Correlation Coefficient	-,647**	-,354	-,344	,918**	,661**	1,000	,562*
	Sig. (2-tailed)	,003	,137	,149	,000	,002	.	,012
Age	Correlation Coefficient	-,415	-,462*	-,577**	,366	,679**	,562*	1,000
	Sig. (2-tailed)	,078	,046	,010	,123	,001	,012	.

*. Correlation is significant at the 0.05 level (2-tailed).

**. Correlation is significant at the 0.01 level (2-tailed).

Appendix H – Supplementary micro-CT results

Control Sample #	*vBMD (g/cm^3)*	*TMD (g/cm^3)*
1	0.993	1.1144
2	0.965	1.13
3	0.840	1.0921
4	0.895	1.0173
5	0.910	1.1216
6	1.157	1.2607
7	1.070	1.1769
8	0.840	1.0539
9	1.064	1.2014
10	0.874	1.0652
11	0.871	1.075
12	1.068	1.2503
13	0.868	1.073
14	0.815	1.0658
15	1.079	1.2661
16	1.020	1.1761
17	0.955	1.1389
18	0.621	0.9813
19	1.103	1.2084
20	0.781	1.0257
21	0.936	1.144
22	0.866	1.0653
23	0.847	1.0876
24	1.195	1.3351

OI Sample #	*vBMD (g/cm^3)*	*TMD (g/cm^3)*
1	0.687	1.0708
2	0.909	1.2051
3	0.871	1.1416
4	0.975	1.1549
5	0.674	0.9991
6	1.079	1.276
7	0.762	1.1306
8	0.719	1.0568
9	0.718	1.0464
10	0.722	1.051
11	1.082	1.1842
12	0.915	1.2791
13	1.110	1.3608
14	0.680	1.0979
15		
16	0.850	1.1541
17		
18	0.604	1.0
19	0.683	1.0636

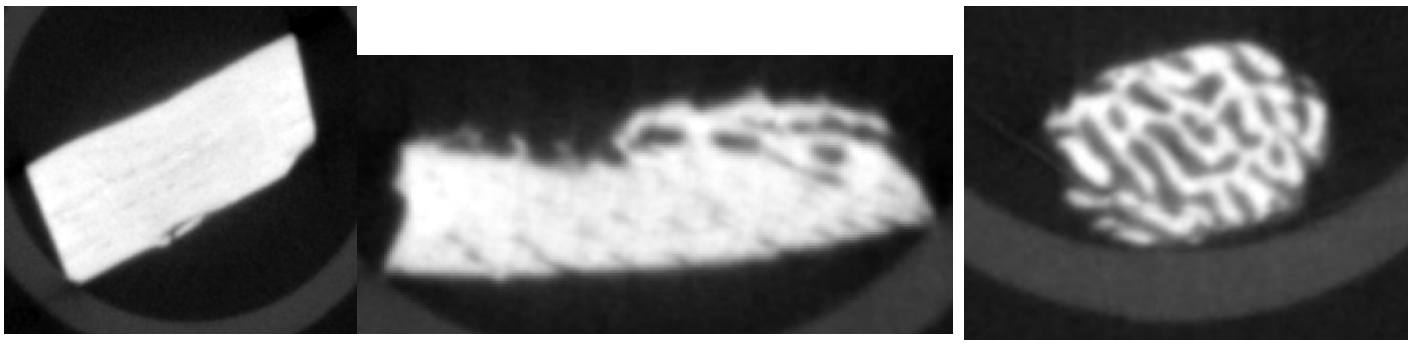

Figure 17. *µCT images of three different cortical bone samples.* ***(Left)*** *Fragment of dense control bone.* ***(Middle)*** *Fragment of OI cortical bone.* ***(Right)*** *Fragment of woven-like cortical OI bone.*

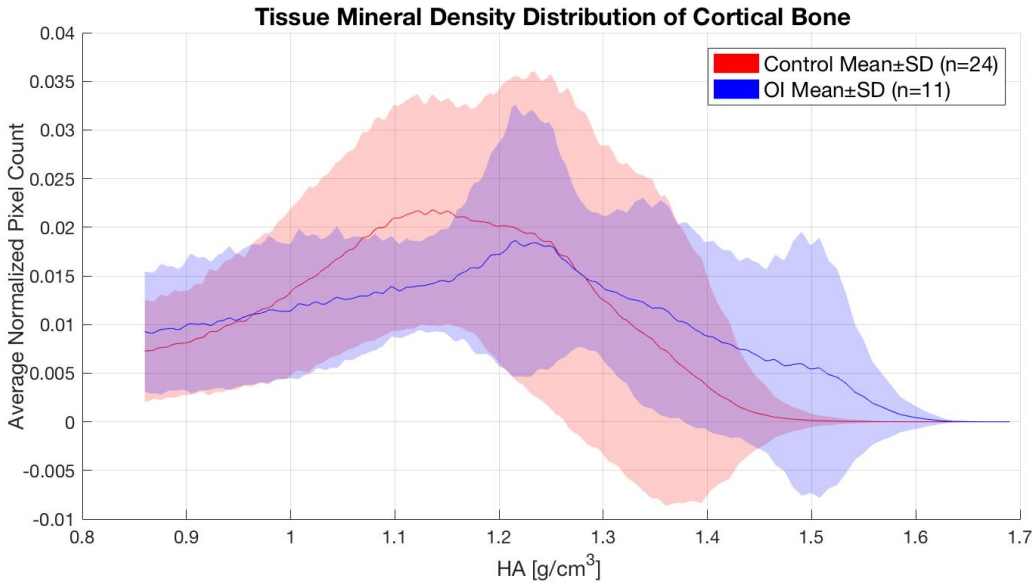

Figure 18. *Tissue mineral density distribution of cortical bone samples. Woven-like cortical bone samples are excluded. In every sample, the frequency of each voxel density is counted and normalized over the total amount of measured voxels. The mean of all individual samples for each density is shown in this diagram. The red line represents the average voxel density in control bones, and the blue line is the mean of the OI samples. Red or blue shading around the line shows 1 SD above and below the mean.*

Appendix I – Supplementary indentation results

Young's Modulus	*Age*
OI-all	(ρ = 0.378, p = 0.149)
OI-type III	(ρ = 0.471, p = 0.143)
Control	(ρ = 0.166, p = 0.497)

Hardness	*Age*
OI-all	(ρ = 0.253, p = 0.343)
OI-type III	(ρ = 0.247, p = 0.464)
Control	(ρ = 0.234, p = 0.334)

Spearman correlations between Young's modulus or hardness versus age.

Spearman correlations: **OI**		Hardness	Young's Modulus	vBMD	vTMD
vBMD	Correlation Coefficient	,491	,444	1,000	,887**
	Sig. (2-tailed)	,053	,085	.	,000
vTMD	Correlation Coefficient	,362	,447	,887**	1,000
	Sig. (2-tailed)	,169	,083	,000	.
Collagen	Correlation Coefficient	,215	,112	-,314	-,551*
	Sig. (2-tailed)	,425	,680	,220	,022
Hyl/Collagen	Correlation Coefficient	-,085	-,118	-,569*	-,534*
	Sig. (2-tailed)	,753	,664	,017	,027
HP/LP ratio	Correlation Coefficient	-,459	-,503*	-,436	-,451
	Sig. (2-tailed)	,074	,047	,080	,069
HP/Collagen	Correlation Coefficient	-,047	-,197	,179	,294
	Sig. (2-tailed)	,863	,464	,492	,252
LP/Collagen	Correlation Coefficient	,382	,374	,463	,525*
	Sig. (2-tailed)	,144	,154	,061	,031
HP+LP/Collagen	Correlation Coefficient	,068	-,026	,275	,451
	Sig. (2-tailed)	,803	,922	,286	,069

Spearman correlation: **CONTROLS**		Hardness	Young's modulus	vBMD	vTMD
vBMD	Correlation Coefficient	,212	,288	1,000	,901**
	Sig. (2-tailed)	,383	,232	.	,000
vTMD	Correlation Coefficient	-,019	,193	,901**	1,000
	Sig. (2-tailed)	,937	,429	,000	.
Collagen/Bone	Correlation Coefficient	-,005	-,193	-,532**	-,561**
	Sig. (2-tailed)	,983	,429	,007	,004
Hyl/Collagen	Correlation Coefficient	-,509*	-,621**	-,253	-,356
	Sig. (2-tailed)	,026	,005	,233	,088
HP/LP ratio	Correlation Coefficient	,161	,012	-,236	-,415*
	Sig. (2-tailed)	,509	,960	,268	,044
HP/Collagen	Correlation Coefficient	-,116	,009	,322	,277
	Sig. (2-tailed)	,637	,972	,125	,189
LP/Collagen	Correlation Coefficient	-,188	,007	,324	,440*
	Sig. (2-tailed)	,442	,977	,122	,031
HP+LP/Collagen	Correlation Coefficient	-,098	,044	,436*	,446*
	Sig. (2-tailed)	,689	,858	,033	,029

*. Correlation is significant at the 0.05 level (2-tailed). **. Correlation is significant at the 0.01 level (2-tailed).

Appendix J – Correlations in control samples

Figure 19. In the images below, significant correlation lines are plotted for CONTROL samples. OI data points are included in the images to show differences.

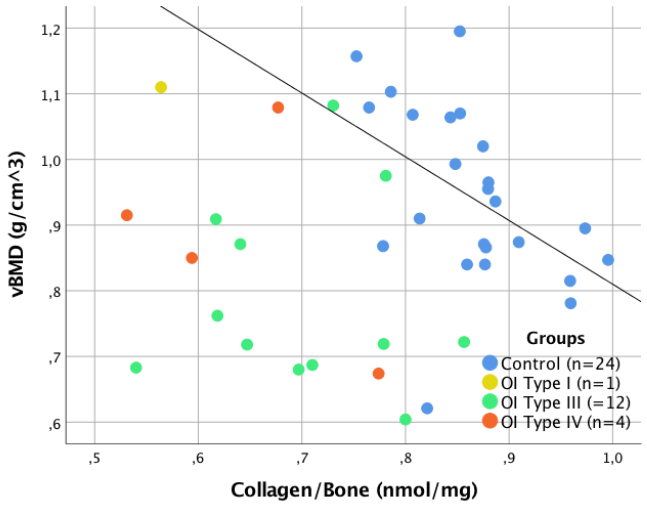

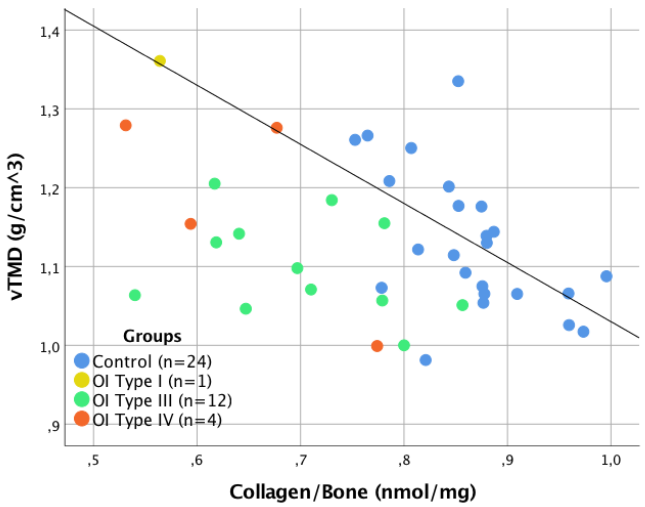

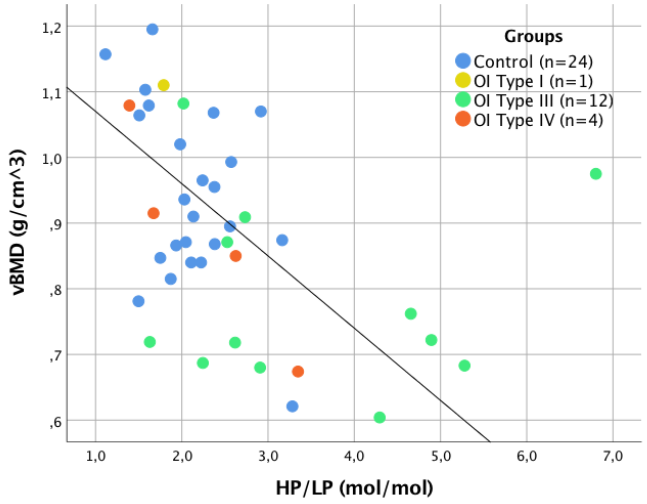

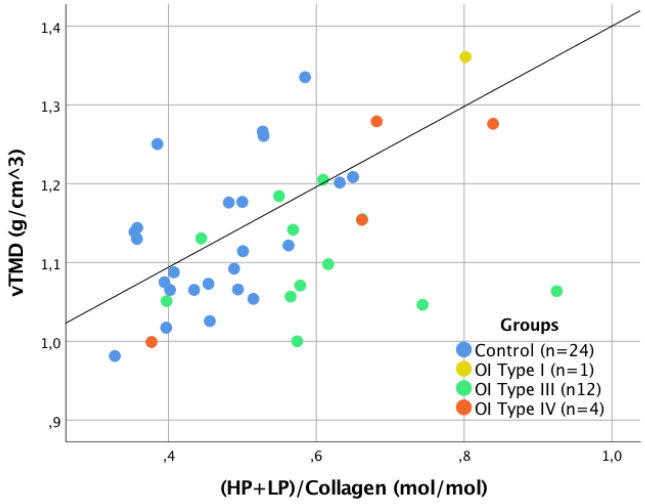

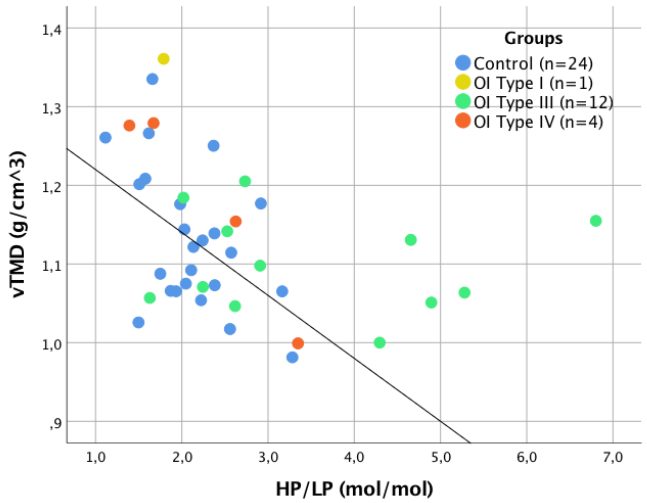

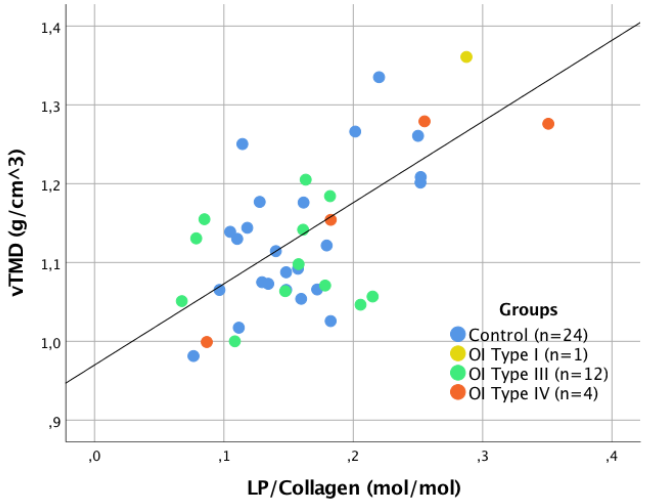

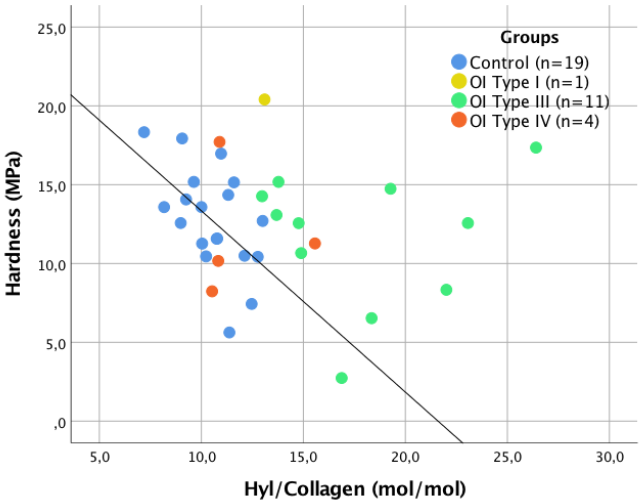
Groups
Control (n=19)
OI Type I (n=1)
OI Type III (n=11)
OI Type IV (n=4)
Hardness (MPa)
25,0
20,0
15,0
10,0
5,0
,0
5,0
10,0
15,0
20,0
25,0
30,0
Hyl/Collagen (mol/mol)

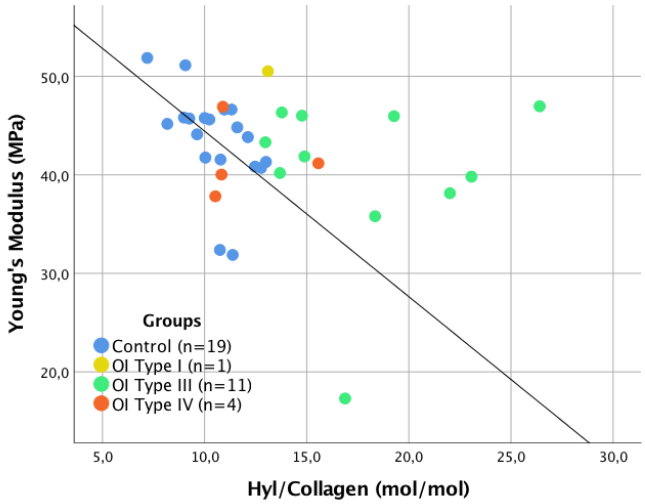
Young's Modulus (MPa)
50,0
40,0
30,0
20,0
Groups
Control (n=19)
OI Type I (n=1)
OI Type III (n=11)
OI Type IV (n=4)
5,0
10,0
15,0
20,0
25,0
30,0
Hyl/Collagen (mol/mol)

Appendix K – Correlations in OI samples

Figure 20. In the images below, significant correlation lines are plotted for OI samples. Control data points are included in the images to show differences.